EFFECTS OF THERMAL OXIDATION OF GAMMA TITANIUM ALUMINIDE ON HUMAN OSTEOBLAST ADHESION

by

SAMIR ALEJANDRO BELLO MELO

A thesis submitted in partial fulfillment of the requirements for the degree of

MASTER OF SCIENCE
in
BIOLOGY

UNIVERSITY OF PUERTO RICO
MAYAGÜEZ CAMPUS
March, 2009

Approved by:

_____	_____
Vivian Navas Almeyda, Ph.D. Member, Graduate Committee	Date
_____	_____
Paul A. Sundaram, Ph.D. Member, Graduate Committee	Date
_____	_____
Anthony Valance Washington, Ph.D. Member, Graduate Committee	Date
_____	_____
Nanette Diffoot-Carlo, Ph.D. President, Graduate Committee	Date
_____	_____
Teodoro Ruiz, Ph.D. Representative of Graduate Studies	Date
_____	_____
Nanette Diffoot-Carlo, Ph.D. Chairperson, Biology Department	Date

ABSTRACT

The corrosion resistance of gamma titanium aluminide (gamma-TiAl), a potential implant material, is increased *in vitro* by thermal oxidation. Although the biocompatibility of autoclaved gamma-TiAl was previously demonstrated, the osteoblast response to thermally oxidized gamma-TiAl has not been addressed to date. Thus, the adhesion of human osteoblasts to oxidized gamma-TiAl surfaces was examined *in vitro.* Cell adhesion on thermally oxidized Ti-6Al-4V was evaluated for comparison. hFOB 1.19 cells were seeded on autoclaved (GTi, TiV), thermally oxidized at 500ºC (GTi5, TiV5), and at 800ºC (GTi8, TiV8) gamma-TiAl and Ti-6Al-4V disks, respectively. A hexosaminidase assay, Scanning Electron Microscopy (SEM) and immunofluorescent labeling of β1 integrin and vinculin were used to evaluate cell adhesion on the different surfaces. Hexosaminidase assay showed no differences in cell attachment on all surfaces 1 day postseeding, but fewer cells were attached on TiV8 compared to those attached on the other surfaces, 7 and 14 days postseeding. Expression of β1 integrin and vinculin in cells cultured for 7 days on all the surfaces, except on TiV8, was demonstrated by immunofluorescent labeling. SEM images showed that cells adhered on all but TiV8 surfaces, 14 days postseeding. Taken together, the results indicate that hFOB 1.19 cells were able to attach and proliferate on autoclaved and both thermally oxidized gamma-TiAl surfaces in a similar manner, suggesting its biocompatibility. On the contrary, TiV8 surfaces exhibit cytotoxic effects on hFOB 1.19 cells in a time dependent manner.

RESUMEN

La resistencia a la corrosión de gama titanio aluminio (gamma-TiAl), un potencial material de implante, se incrementa *in vitro* mediante oxidación térmica. Aunque anteriormente se demostró la biocompatibilidad del gamma-TiAl autoclaveado, la respuesta de los osteoblastos a las superficies de gamma-TiAl oxidadas térmicamente no se ha abordado hasta la fecha. Por esto, examinamos *in vitro* la adhesión de osteoblastos humanos a la superficie de gamma-TiAl oxidado térmicamente. Se evaluó la adhesión celular en la aleación Ti-6Al-4V oxidada térmicamente con fines comparativos. Células hFOB 1.19 fueron sembradas sobre discos autoclaveados (GTi, TiV) y oxidados térmicamente a 500ºC (GTi5, TiV5) o a 800ºC (GTi8, TiV8) de gamma-TiAl y Ti-6Al-4V, respectivamente. Un ensayo de hexosaminidasa, Microscopia Electrónica de Rastreo (MER) y marcaje inmunofluorescente de integrina β1 y vinculina se usaron para evaluar la adhesión celular en las diferentes superficies. El ensayo de hexosaminidasa no mostró diferencias significativas en la adhesión celular en todas las superficies evaluadas 1 día post-siembra, pero menos células se adhirieron sobre TiV8 comparado al número de células adheridas sobre las otras superficies, 7 y 14 días post-siembra. Se demostró mediante marcaje inmunoflorescente la expresión de integrina β1 y de vinculina en las células cultivadas por 7 días sobre todas las superficies, excepto en TiV8. Las imágenes de MER mostraron células adheridas en todas las superficies, excepto en TiV8, 14 días post-siembra. En conjunto, los resultados indican que las células hFOB 1.19 fueron capaces de adherirse y proliferar sobre las superficies de gamma-TiAl autoautoclaveadas y oxidadas térmicamente de forma similar, sugiriendo su biocompatibilidad. Por el contrario, las superficies de TiV8 exhiben efectos citotóxicos sobre las células hFOB 1.19 en una manera dependiente del tiempo.

To my lovely parents Alcides and Blanca, I miss you.

To my beloved nieces and nephews, I hope to see you soon.

ACKNOWLEDGEMENTS

I want to thank God for giving me the opportunity to successfully finish this stage of my life. During the development of my graduate studies at the University of Puerto Rico several persons collaborated directly and indirectly with my research. That is why I wish to dedicate this section to recognize their support.

I want to start by expressing a sincere acknowledgement to my advisor, Dr. Nanette Difoot-Carlo for giving me the opportunity to work under her guidance and supervision, and for the critical reading of the thesis. I also want to thank the motivation and support I received from Dr. Vivian Navas-Almeyda and Dr. Paul A. Sundaram, members of my Graduate Committee, who always encouraged me to finish my work in spite of the difficulties encountered in the way. A special gratitude to Dr. Anthony Valance Washington, member of my Graduate Committee, for the critical reading of the thesis and for his disposition to participate in my oral examination.

I deeply appreciate the support in statistics and transmitted knowledge of Dr. Damaris Santana Morant, Professor of the Department of Mathematical Sciences and Coordinator of the "Laboratorio de Consultoría Estadística" (LCE) of UPRM. I also want to thank Dr. Mónica Alfaro, Professor of the Department of Biology, who helped me in the editing of the statistical results. Idaris de Jesús, my friend and technician of the Molecular Virology lab, thanks for your optimism and your help with the immunofluorescent experiments. Special mention to my lab partners: Militza, Alexa, Sara, Ixia, Pricilla, Yamilette, Rey, Krystal, Diane and Franklin. Thanks for your support and friendship.

I want to thank Mr. José Almodovar (Tito) and Ms. Jessamine Hernández for their technical assistance in SEM and Confocal Microscopy, and the processing of the metallic disks, respectively. They always demonstrated their disposition in helping me to solve the technical problems encountered in the way. My gratitude to Dr. Arturo Massol and Alejandro Caro for the use of the microplate reader ThermoMax for the hexosaminidase assay. I also want to express my gratitude to my fellow graduate students and friends Diana Saénz, Marcela Díaz, Eduar Guerrero, Azucena Camacho, Zamira Youssef, and Yobana Mariño. Thanks to Roy Morales Burgos for the laughs, the talks, the companionship, the motivation, and his huge generosity. I

also want to thank Héctor Luis Salazar, for his support from far away during my first years in Puerto Rico. At last, I would like to thank my family, for their unconditional support and love.

The Grant SO6GM-08103 from National Institute of General Medical Sciences (NIGMS)/ MBRS-SCORE, University of Puerto Rico, Mayagüez Campus, provided the funding and the resources for the development of this research.

TABLE OF CONTENTS

TABLE LIST

Tables **Page**

FIGURE LIST

Figures **Page**

1 INTRODUCTION

Titanium (Ti) and its alloys have been used as implant materials due to their biocompatibility properties. Although Ti-6Al-4V is the most common titanium alloy used in bone repair and replacement, yet its use as a biomaterial has some constraints. The possibility of vanadium release from Ti–6Al–4V and its low wear resistance are of serious concerns in using this alloy as a biomaterial (1-3). This has led to the study of different Ti alloys without vanadium and with better mechanical properties than Ti–6Al–4V as possible implant materials. New generations of gamma-based TiAl intermetallic alloys have been developed for applications in the automotive and aerospace industries. Gamma-TiAl alloys possess low density (3.8 g/cm^3), high stiffness and mechanical strength (up to 1000 MPa), and good oxidation and corrosion properties (4-5). A preclinical study of Ti-48Al-2Cr-2Nb (at.%) (hereafter referred to as gamma-TiAl), used as implant material on rats, showed cell attachment and bone tissue formation on the alloy, suggesting its biocompatibility (6). Recently, an *in vitro* study reported that growth, attachment and differentiation of human fetal osteoblasts (hFOB 1.19) on gamma-TiAl and Ti-6Al-4V were similar, and not affected by the surface roughness of the metal, suggesting that gamma-TiAl has the potential to be used as implant material (7).

Corrosion is a deteriorating reaction that occurs when metallic materials come in contact with an environment of bodily fluids. Corrosion may lead to undesirable release of metal ions, which potentially may have localized or systemic cytotoxic, genotoxic and even carcinogenic effects *in vivo* (3,58,59). Titanium and its alloys spontaneously form a thin biocompatible surface oxide layer, composed primarily of TiO_2. When the titanium alloy is implanted *in vivo*, the oxide stability may be altered resulting in increased metal ion release and implant failure (7). Several treatments have been developed to modify the surface oxides on Ti alloys to improve their wear resistance. Advanced surface modification methods (e.g. plasma ion implantation), anodizing, ultrapassivation, nitriding, electrochemical and thermal oxidation have been applied to Ti-6Al-4V leading to the formation of stable superficial oxides (3, 8-12). Thermal oxidation treatment induces the formation of thick, highly crystalline oxide films with increased surface roughness, and good protective performances. Some *in vitro* studies have demonstrated that thermal oxidation treatment improves the corrosion resistance and osteoblast adhesion on Ti-6Al-4V alloy (8-14). A recent study showed that the corrosion resistance of gamma-TiAl in Ringer's solution is improved by thermal oxidation (4). In addition, the wear resistance of gamma-TiAl

may be improved by oxidizing this alloy at temperatures that preferentially form a hard alumina surface layer (15). The response of osteoblast cells to gamma-TiAl surface oxides formed by thermal oxidation has not been studied. In this study, the effect of thermal oxidation of gamma-TiAl on osteoblast adhesion was evaluated *in vitro*. The results of this study are important to know if thermal oxidation could be a treatment recommended for gamma-TiAl if it is used as implant material.

The human fetal osteoblast cell line (hFOB 1.19), an established cell line, was used to evaluate cell adhesion on gamma-TiAl disks. These cells are immortalized and can be subcultured for a long period of time. In addition, they have the ability to differentiate into mature osteoblasts (16-19). The changes in morphology of the hFOB 1.19 cells throughout different time periods of culture have not been studied. To establish a baseline for comparison purposes, cell morphology on glass coverslips was observed at different incubation time points (1, 3, 5, 7,14, 21 and 28 days) using Scanning Electron Microscopy (SEM). The data obtained was used to compare the osteoblast cells cultured on the different surfaces used in this research, and to determine if surface oxides formed on gamma-TiAl and Ti-6Al-4V affect the morphology and the differentiation of hFOB 1.19 cells.

2 LITERATURE REVIEW

2.1 BONE COMPOSITION

Bone is a vascular connective tissue that consists of cells (osteoprogenitor cells, osteoblasts, bone lining cells, osteocytes, and osteoclasts), and a mineralized extracellular matrix (ECM). Calcified bone contains about 25% organic matrix, 5% water, and 70% inorganic mineral. The mineral is calcium phosphate, in the form of hydroxyapatite crystals [$Ca_{10}(PO_4)_6(OH)_2$]. Osteoid, the non- mineralized extracellular matrix, is composed of 90% collagenous proteins (97% type I collagen. 3% type V collagen, and trace amounts of others types of collagens), and of 10% noncollagenous proteins. The four main groups of noncollagenous proteins found in the bone matrix are multiadhesive glycoproteins, proteoglycans, bone-specific vitamin K-dependent proteins, growth factors and cytokines (19-23).

The multiadhesive glycoproteins are in charge of attachment of bone cells and collagen fibers to the mineralized matrix. Some of the more important glycoproteins are osteonectin, osteopontin and sialoproteins I and II. The proteoglycans contribute to the compressive strength of the bone and are responsible for binding growth factors and may inhibit mineralization. Osteocalcin (which captures calcium from the circulation and stimulates osteoclasts), protein S, and matrix Gla-protein are some of the more important bone specific vitamin K-dependent proteins. The growth factors and cytokines include small regulatory proteins like bone morphogenetic proteins (BMPs), interleukins, insulin-like growth factors (IGFs). The bone extracellular matrix has several functions, such as support, protection, a calcium and phosphate reservoir and in homeostasis (19-23).

Different cell types are associated with bone. Osteoprogenitor cells are cells derived from mesenchymal stem cells; they give rise to osteoblasts. Osteoblasts are the cells found on bone surfaces that lay down the extracellular matrix and regulate the bone mineralization. The calcification process appears to be initiated by the osteoblasts through secretion into the matrix of small, 50 to 250 nm, membrane- limited matrix vesicles that are rich in alkaline phosphatase. The osteoblasts are cuboidal or polygonal cells with a round nucleus, a prominent Golgi complex and abundant rough endoplasmic reticulum. Osteoblasts usually are found in a single layer adherent to periosteal or endosteal surfaces of the bone. These cells are highly anchorage dependent and rely on extensive cell–matrix and cell–cell contacts via a variety of

transmembranous proteins (integrins, connexins, cadherins) and specific receptors (for cytokines, hormones, growth factors) to maintain cellular function and responsiveness to metabolic and mechanical stimuli. The lifespan of a human osteoblast is estimated between 2 and 3 months, during which time it lays down 0.5–1.5 μm osteoid per day. Some osteoblasts may become incorporated as osteocytes in their own calcified matrix, and others may remain as bone lining cells when there is no active growth (19-21, 23).

Osteocytes are the most abundant cells in bone (making up 95% of bone cells). These cells are responsible for maintaining the bone matrix. They respond to mechanical forces applied to bone (mechanotransduction) synthesizing new matrix or participating in matrix degradation. Death of osteocytes, either through trauma, cell senescence, or apoptosis results in reabsorption of the bone matrix by osteoclast activity, followed by repair or remodeling of the bone tissue. Osteocytes are typically smaller than osteoblasts because of their reduced perinuclear cytoplasm (contain less cell organelles associated with protein synthesis than osteoblasts). Osteocytes have a higher number of cytoplasmatic extensions (filopodia), which serve to interconnect the osteocytes and to connect them with the osteoblasts. Osteocytes are found in peri-cellular lacunae, which are small independent regions surrounding each cell. These cells are not capable of division and are lost when the bone in which they reside is degraded, for which reason the lifespan of an osteocyte depends on the lifespan of the bone (19-21, 23).

Osteoclasts have the ability to reabsorb mineralized bone at sites called Howship's lacunae (resorption bays). These cells are derived from fusion of mononuclear hematopoietic progenitor cells called CFU-GM. Osteoclasts are highly migratory, multinucleated, and polarized cells which carry an arsenal of lysosomal enzymes. These cells form a tight seal with the calcified matrix by means of the apical membrane (ruffled cell border), and secrete the lysosomal enzymes to the subosteoclastic space formed, thus originating the resorption bays. Proton pumps present in this region of the membrane lower the pH to values between 2 and 4, activating the secreted enzymes especially tartrate-resistant acid phosphatase (TRAP), cathepsin K (cysteine protease) and matrix metalloproteinases. The acidic environment initiates the degradation of the mineral component of bone to calcium ions, soluble inorganic phosphates, and water. An activated osteoclast is capable of reabsorbing 200000 μm^3/day. When bone reabsorption is completed, osteoclasts undergo apoptosis. The lifespan of an osteoclast is thought to be in the range of 4 to 6 weeks (19-21, 23).

2.2 HUMAN OSTEOBLAST CELL LINE hFOB 1.19

Human osteoblast cell line hFOB 1.19 was established by transfection of fetal bone-derived osteoblast cells with a gene coding for a temperature-sensitive mutant (tsA58) of the SV40 T antigen along with a gene coding for neomycin (G418) resistance (36). Cells grown at a permissive temperature of 33.5°C exhibit rapid cell division (doubling time of ~36 hrs), whereas little cell division occurs at elevated (38°C) temperature (doubling time of ~96 hrs). The hFOB 1.19 clone can be cultured at 33.5°C up to passage 30 (~100 population doublings) without crisis. At passage 32-34 the cells enter crisis and proliferation slows considerably (17). At the restrictive temperature (39.5°C) hFOB 1.19 cells do not proliferate, leading to a steady decrease in cell numbers. Differentiation increases and a more mature osteoblast phenotype is produced in post-confluent cultures incubated at 33.5°C, or in cultures (independent of their confluency level) incubated at the restrictive temperature. Phenotypic markers of osteoblasts differentiation of the cell line hFOB 1.19 include expression of alkaline phosphatase, osteopontin, osteonectin, osteocalcin, bone sialoproteins, and type I collagen. Furthermore, this cell line exhibits an increase in cellular cAMP levels in response to parathyroid hormone (PTH), an increase in osteocalcin levels in response to dihydroxyvitamin D_3 treatment, and the formation of a mineralized matrix. This cell line also sustains minimal karyotype damage and maintains its anchorage-dependence for growth even after multiple passages (17-19).

Different osteoblastic cell lines have been used for studying cell adhesion on potential biomaterials *in vitro*. The most widely used cells are primary osteoblasts derived from normal human and rodent bone fragments, or osteosarcoma cell lines generated from human bone tumors. Each of these cell sources has strengths and limitations. The primary-human osteoblast cultures are an excellent normal source of cells but their heterogeneity of phenotype and stage of differentiation, a slow growth rate, and limited life span in culture represent limitations when used. Rodent cultures generally circumvent these problems but may not be appropriate models for humans due to trans-species differences in phenotypic characteristics. The use of transformed human osteosarcoma cell lines is limited because they do not exhibit the complete phenotype of differentiated osteoblasts, have abnormal growth properties, and exhibit response to hormones and cytokines that sometimes differ from those of primary cultures (17-19). Since hFOB 1.19 cells have the ability to differentiate into mature osteoblasts and can be subcultured for a long period of time due to their immortality, they constitute a valuable option in research related to

bone replacing materials (17-19). This cell line has been used to study the effects of the surface characteristics of different substrata on osteoblast phenotypic responses (25-26).

2.3 METALLIC BIOMATERIALS

A biomaterial is a nonviable material used in a medical device, intended to interact with biological systems (27). These materials are implanted in the human body for the purposes of promoting improved human health (27, 28). Biocompatibility is the ability of a material to perform with an appropriate host response in a specific application (27). Metallic biomaterials for implantable medical devices have fundamental mechanical integrity and biocompatibility requirements. The mechanical integrity requirements include resistance to permanent deformation under monotonic loading, resistance to crack initiation and propagation, and resistance to wear. The biocompatibility requirements include those that focus on the effects of the physiological environment on the *in vivo* performance of the implant itself as well as the effects of the implant on local and systemic tissue (27).

Metals have been successfully used as biomaterials for many years. Their most important applications have been in orthopedics (e.g., total joint prostheses), oral and maxillofacial surgery (e.g., dental implants, craniofacial plates and screws) and cardiovascular surgery (e.g., parts of pacemakers, defibrillators, and artificial hearts; valve replacements). For structural applications in the body (e.g., implants for hip, knee, ankle, shoulder, wrist, finger, or toe joints), the principal metals are stainless steels, cobalt-base alloys, and titanium-base alloys. The ideal alloy would have the modulus of magnesium, the strength of cobalt-chromium alloys, the corrosion resistance and biocompatibility of titanium, and the fabricability of stainless steel (28).

Stainless steels are iron-base alloys that contain a minimum of 10.5% chromium (Cr), the amount needed to prevent the formation of rust in unpolluted atmospheres. They achieve their stainless characteristics through the formation of an invisible and adherent chromium-rich oxide surface film (~2 nm thick). The addition of nickel and an increase in the Cr content beyond the minimum of 10.5% confers still greater corrosion resistance. The addition of other alloying elements may be used to enhance resistance to specific corrosion mechanisms or to develop desired mechanical and physical properties. Austenitic stainless steels are popular for implant applications because they are relatively inexpensive, they can be formed with common techniques, and their mechanical properties can be controlled for optimal strength and ductility.

Nevertheless, these alloys are not sufficiently corrosion resistant for long-term use as an implant material. They find use as bone screws, bone plates, intramedullary nails and rods, and other temporary fixation devices. Recently, nitrogen strengthened stainless steels alloys have been developed. These alloys, which have increased corrosion resistance and improved mechanical properties, are being used for bone plates, bone screws, spinal fixation components, and other medical components (27, 28).

The cobalt based alloys display a useful balance between mechanical properties and biocompatibility, being superior to stainless steel in strength and corrosion resistance, but more expensive to manufacture. The corrosion resistance of cobalt-chromium (Co-Cr) alloys is more than an order of magnitude greater than that of stainless steels. The two Co-Cr alloys predominantly used as implant alloys are cobalt-chromium-molybdenum (Co-Cr-Mo) and cobalt-nickel-chromium-molybdenum (Co-Ni-Cr-Mo). Other Co-based alloys approved for implant use include one that incorporates tungsten (Co-Cr-Ni-W) and another with iron (Co-Ni-Cr-Mo-W-Fe). These four Co-based alloys can be divided into two main types by the manufacturing condition: cast alloy or wrought alloy. Co-Cr-Mo (commonly known as Vitallium or Haynes 21) is a cast alloy and the other three are wrought alloys. The main attribute of Co-Cr-Mo alloys is corrosion resistance in chloride environments, which is related to its high chromium content and the surface oxide (Cr_2O_3). This alloy cannot be contoured at the time of surgery because of its high rate of work hardening. Accordingly, this alloy is typically reserved for implantable devices having a fixed configuration (e.g., total hip prosthesis). In addition, because of its high abrasion resistance, it is sometimes used for bearing applications such as metal-on-metal total joint devices (27, 28).

In the past 20 years titanium and its alloys have gained more attraction as biomaterials due to their lower modulus, superior biocompatibility, and enhanced corrosion resistance when compared to more conventional stainless steels and cobalt-based alloys. Titanium is a low density element that can be highly strengthened by alloying and deformation processing. Titanium and its alloys used for implant devices have been designed to have excellent biocompatibility, with little or no reaction with tissue surrounding the implant. Titanium derives its corrosion resistance from the stable oxide film that forms on its surface, which can reform at body temperatures and in physiological fluids if damaged. Titanium is a transition metal with an incomplete shell in its electronic structure that enables it to form solid solutions with most

substitutional elements having a size factor within ± 20%. In its elemental form titanium has a high melting point (1678°C), exhibiting an hexagonal close packed crystal structure (hcp) up to the beta transus (882.5°C), transforming to a body centered cubic structure (bcc) β above this temperature. Titanium alloys may be classified as either α, near-α, α + β, metastable β or stable β depending upon their room temperature microstructure. Alloying elements for titanium fall into three categories: α- stabilizers (Al, O, N, and C), β- stabilizers (Mo, V, Nb, Ta, Fe, W, Cr, Si, Ni, Co, Mn, and H), and neutral (Zr) (29, 30).

Ti-6Al-4V is one of the most commonly used titanium alloys. This is an α + β alloy containing 6% Aluminum and 4% Vanadium. This alloy exhibits an excellent combination of corrosion resistance, strength, low modulus of elasticity, and toughness. Typical applications include medical devices, implants, aerospace applications, and pressure vessels. The microstructure of Ti-6Al-4V alloy depends on thermo-mechanical processing. If the alloy is heated and worked at temperatures near but not exceeding the beta transus, and then annealed, a microstructure of fine-grained alpha with beta as a second phase at grain boundaries can be produced. If the alloy is heated into the beta phase field (above 1000°C) and is then cooled slowly to room temperature, two phases are obtained, large beta grains and platelet alpha structure with grains. This kind of titanium alloy is widely used for total joint replacement arthroplasty (primarily hips and knees) application. Despite their excellent mechanical properties, Ti-6Al-4V alloys have poor shear strength and cause seizing because of high coefficients of friction, both in bone-metal and metal-metal interfaces (19). Furthermore, their clinical use has some concerns due to problems caused by the release of vanadium (V) from Ti-6Al-4V alloys. V has been reported to be toxic and shows adverse tissue effects (18). Consequently, new titanium alloy compositions were developed. Among these are the gamma titanium aluminide alloys.

Gamma titanium aluminide (gamma-TiAl) is an intermetallic material commonly used in applications where high temperature is required (aerospace and automotive applications). This alloy has excellent properties compared to Ti-6Al-4V. Gamma-TiAl offers superior corrosion resistance, high specific strength and rigidity, and a lower density (3.8 g/cm^3) compared to Ti-6Al-4V (4.42 g/cm^3) (4-7, 30). In addition, this new material is proposed to possess excellent biocompatibility and good long-term fatigue and wear properties. These characteristics make gamma-TiAl very attractive for high temperature applications in aggressive environments as well as for endoprothesic applications (5). In these kinds of alloys there is the possibility of modifying

the composition to obtain specific biomedical applications. Common compositions of gamma-TiAl are Ti-48Al-2Cr-2Nb and Ti-46.5Al-4(Cr-Nb-Ta)-0.1B. Gamma-TiAl alloys commonly used are in the range Ti-(46-52)Al-(1-10) M, where M is at least one element from V, Cr, Mn, Nb, Ta, W and Mo. These alloys can be divided into single phase (γ) and two-phase (γ + α2) alloys (4, 5, 30).

Gamma-TiAl alloy Ti-48Al-2Cr-2Nb was evaluated as implant material using an *in vivo* rat model to study its biocompatibility (6). Sprague-Dawley rats were implanted with gamma-TiAl cylinders in the femur and observed for an experimental period lasting up to 180 days. Using SEM, bone formation and maturation over implants were observed as early as 45 days post-implantation suggesting outstanding biocompatibility. Implants were completely covered with cortical bone tissue 180 days post-implantation. At this time, neither signs of rejection nor inflammatory responses were observed around gamma-TiAl implants. In addition, the bone-metal interfaces showed signs of tissue growth from the original bone to the metal surfaces (6).

In vitro biocompatibility of the gamma-TiAl alloy Ti-48Al-2Cr-2Nb, using fetal human osteoblasts (hFOB 1.19) was recently evaluated (7). Using SEM it was shown that osteoblast cells hFOB 1.19 grew and attached on gamma-TiAl, and on Ti-6Al-4V (control alloy) in a similar manner. The study determined that the surface roughness (polished with 600 grit, 3μ diamond and Mastermet) had no effects on osteoblast growth, attachment and proliferation on gamma-TiAl and Ti-6Al-4V alloys. Immunofluorescent labeling assays demonstrated the synthesis of ECM components (collagen type I and osteonectin) by human osteoblasts cultured on both gamma-TiAl and Ti-6Al-4V surfaces, suggesting that gamma-TiAl alloy has the potential to be used as implant material.

2.4 OSTEOBLAST ADHESION TO MATERIALS

Orthopedic or dental implants osseointegrate if they establish a mechanically solid interface with complete fusion between the material's surface and the bone tissue with no soft tissue interfaces. Implant osseointegration depends on the material biocompatibility, and this property is closely related to cell behavior on contact with biomaterial, particularly cell adhesion to its surface. The term "adhesion" in the biomaterial domain includes the attachment and the adhesion phases. The first phase includes short-term events such as physicochemical linkages between cells and materials involving ionic forces, van der Waals forces, etc. The second phase

consists of long-term linkages between cells and materials by means of ECM proteins, cell membrane proteins, and cytoskeleton proteins (23, 31).

When an implant material is placed in a defect (*in vivo*) or in culture medium (*in vitro*), its surface will be coated with either blood or serum proteins, respectively. Cells that express integrins (cell membrane receptors) are able to adhere to implant surfaces covered with ECM proteins, originating from blood or serum. These proteins are adhesive because they contain sequences like Arg-Gly-Asp (RGD) and Asp-Gly-Glu-Ala (DGEA), which are specific to the fixation of integrins (32-36). Geiβler *et al.* (36) evaluated the osteoblast adhesion on collagen type I coated Ti6Al4V disks. They used as control groups uncoated Ti6Al4V disks and polystyrene. Their results suggest that DGEA was the sequence recognized by the osteoblast receptors on collagen type I coated Ti6Al4V disks, whereas RGD was the sequence recognized by osteoblast on non-collagen coated Ti6Al4V and polystyrene materials. Kornu *et al.* (37) determined that although osteoblast cells are able to adhere to titanium and cobalt alloys in serum-free medium, maximal osteoblast binding require serum proteins. They observed that fibronectin pretreatment of the metallic alloys increased cell attachment 2.6-fold.

The sites of adhesion between osteoblasts and substrate surfaces are called focal adhesions or focal contacts. At these sites, bundles of actin filaments are anchored to receptors of the integrin family through a multi-molecular complex of junctional plaque proteins. The components of focal adhesions are diverse and include scaffolding molecules (e.g., talin, paxillin, vinculin); GTPases, and enzymes (e.g., kinases, phosphatases, proteases, and lipases) (23, 38-40).

Integrins are the major transmembrane components of the focal adhesions. They form a large family of αβ heterodimeric transmembrane receptors involved in adhesion to extracellular matrix components and substrates (31,35,39,41). There are at least eight β-subunits which show strong homology (40-48%) to each other and 18 α-subunits which exhibit less sequence conservation. The pairing of particular α and β subunits confers specificity for a given ECM ligand. Integrin subunits have an extensive extracellular domain, a transmembrane domain and a short cytoplasmic domain. The length of the β chain is around 798 amino acids, with a cytoplasmic region of 20-50 amino acids, and a transmembranous part of 26-29 amino acids. The N-terminus is in the extracellular domain. Integrins interact with the ECM through their extracellular domains, and with components of the cytoskeleton and signaling molecules through their intracellular domains. Through these interactions, integrins can regulate many cellular

functions like cell adhesion, motility, shape, growth, and differentiation (31,35,39). In addition, integrin-mediated adhesion and signaling are responsible for anchorage dependence of growth and cell survival. When anchorage-dependent cells are not able to attach to substrates, they arrest its proliferation and undergo apoptosis (42).

Osteoblasts are capable of expressing a wide variety of integrins. They have been shown to express integrin subunits α1, α2, α3, α4, α5, α6, αv, β1, β3, and β5 (31,32). However, integrin expression is not constant but can vary with the stage of the development of the osteoblast, the cell source, *in vivo* versus *in vitro* characterization, and cell culture substrata (20,21,25,31,32,41) Lim *et al.* (25) found that hFOB 1.19 cells, when cultured either on hydrophilic or hydrophobic surfaces, express integrin subunits α2, α3, α4, α5, αv, β1, and β3, regardless of the substrata examined. However, the relative abundance of the expression was affected by the substratum surface energy (25).

The β1 subunit of integrins is able to interact with at least ten different α subunits. Alternative RNA processing of the β1 subunit results in functionally different subunits with distinct cytoplasmic domains, with β1A being the most common isoform. The β1 subunit seems to be the predominant receptor that mediates osteoblast adhesion to collagen and laminin and in some extent to fibronectin, constituting the main β subunit in osteoblasts. In addition, integrin β1 -mediated interactions promote osteoblast differentiation (43). β1 subunit has been used as an osteoblast adhesion marker in biocompatibility studies of metallic and polymeric materials (9,44-46). Using immunolabeling assays, Anselme *et al.* (44) compared the expression of some adhesion proteins by human osteoblasts cultured for 1, 7 or 14 days on different substrates with the same surface topography. They found that the β1 integrin subunit was expressed on all tested surfaces at each time point. β1 integrin subunits appeared as thin focal contact-like patches as well as thin filaments. They concluded that human osteoblasts attach in a similar manner to substrates with various surface compositions but the same surface topography. Anselme *et al.* (45) evaluated the expression of various adhesion proteins by osteoblasts cultured for 1, 7 or 14 days on rough or polished Ti-6Al-4V surfaces, using immunofluorescence. They found that the integrin β1 subunit was expressed by osteoblasts on rough and polished Ti-6Al-4V surfaces at each time point. However, they observed a decrease in the expression of this protein at day 14

compared to days 1 and 7, on all tested surfaces. They observed β1 integrin subunits as thin focal contact-like patches as well as thin filaments.

Saldaña *et al.* (9) assessed osteoblast adhesion on polished (non-oxidized) and thermally oxidized (at 500°C or 700°C, 1h) Ti-6Al-4V surfaces at 0.5, 1, 1.5, 2, 3, and 24h. They evaluated the β1 integrin and Focal Adhesion Kinase (FAK) - Y397 expression using flow cytometry and immunolabeling assays, respectively. Flow cytometric analysis could not detect any difference in the percentage of cells expressing β1 on the different surfaces at 0.5, 1, 2, 3, and 24h. However, they detected differences in β1 expression on cells cultured for 1.5 h on all tested surfaces. They found that 46.8% of osteoblasts cultured on polished Ti-6Al-4V, 57.8% of osteoblasts cultured on Ti-6Al-4V oxidized at 500°C, and 71.2% of osteoblasts cultured on Ti-6Al-4V oxidized at 700°C were positive for β1 integrin. They concluded that thermal oxidation enhanced cell adhesion on Ti-6Al-4V surfaces.

Amato *et al.* (46) studied the osteoblast adhesion on the biodegradable synthetic polymer poly-(ε-caprolactone) (PCL), using immunofluorescence labeling. They cultured human osteoblasts on untreated PCL, biofunctionalized PCL (PCL that was covered with arginine-glycine-aspartic acid [RGD] sequences), low-energy irradiated PCL, and biofunctionalized irradiated PCL surfaces. They used as adhesion markers β1 integrin subunit and αvβ3 integrin. After 24h of culture, they determined that expression of the β1 integrin subunit was higher in osteoblasts grown on irradiated PCL, covered or not with RGD groups, compared to cells cultured onto other surfaces. The staining pattern of β1 subunit was diffused on cell surface. At the same point of time, they observed that osteoblasts grown on biofunctionalized irradiated PCL surfaces showed the highest αvβ3 integrin expression. They concluded that cell adhesion was enhanced on irradiated PCL surfaces, while the addition of RGD peptides on PCL did not improve cell attachment (46).

2.5 EFFECTS OF THERMAL OXIDATION OF TITANIUM ALLOYS ON OSTEOBLAST ADHESION

Biocompatibility of titanium and its alloys is mainly due to the reactive oxide layer, typically 4-6 nm thick, which spontaneously forms at room temperature on its surface by the reaction of titanium with oxygen. The superficial oxide layer or passive layer (TiO_2, amorphous or poorly crystallized) confers high stability, chemical inertness, and a high *in vitro* corrosion

resistance in many oxidizing media (14,23,47). However, there is evidence that the *in vivo* conditions can alter the stability of the native form of passive layer increasing the material corrosion, leading to a slow release and accumulation of ions in tissue adjacent to the implant. It has been hypothesized that the adherence of the passive film on alloys surfaces is poor, and it may be disrupted at very low shear stresses (14,29). Sustained release of the underlying metal after disruption of the oxide film, and its reformation, results in the gradual consumption of the material, debris formation, and release of metal ions. The dissolution of titanium into the human body can induce the release of potentially osteolytic cytokines (TNF-α or IL-1β) involved in the aseptic implant loosening (9,12,48,49). Furthermore, *in vitro* studies have shown that ions associated with Ti-6Al-4V alloy inhibited the normal differentiation of bone marrow stromal cells to mature osteoblasts, suggesting that the metal ion release from Ti-6Al-4V may inhibit the bone formation on implant surfaces (48). Particulate and ionic debris resulting from *in vivo* degradation of total joint replacement components are recognized as major factors limiting the longevity of the joint reconstruction (50).

Surface treatment modalities of titanium alloys, such as mechanical blasting, anodizing, ultrapassivation, nitriding, ion implantation, chemical vapor deposition, acid-etching processes, sputtering, sol-gel process and thermal oxidation, have been tested as methods to modify surface oxide composition and thickness. Thermal oxidation treatments (at temperatures above 200°C) originate ceramic coatings, mainly based on rutile, that are thick and highly crystalline with very good protective performances. Increasing temperature and time of oxidation induces the formation of a thicker oxide layer. This treatment has been studied for its possible application in wear and corrosion-resistant technologies or implants (9,12,14,30,51).

The appearance of the gamma-TiAl surface after thermal oxidation varies from grey metallic to yellow. This behavior is attributed to gradually increased saturation of oxygen in the alloy surface. Thermal oxidation of gamma-TiAl at 500°C originates a continuous blue colored oxide layer of predominantly Al_2O_3 (alumina), while at 800°C, a dark yellow oxide layer due to the presence of TiO_2 (rutile) is formed. The scale formed on gamma-TiAl at high temperatures is commonly multilayered. It consists of a mixture of TiO_2 in the outer layer, and a combination of TiO_2 and Al_2O_3 in the middle layer. Escudero *et al.* (5) found that thermal oxidation at 700ºC (24h in air) of the gamma-TiAl alloy of composition Ti-45Al-2W-0.6Si-0.7B (at.%) originates a thin Al_2O_3 layer and at 1000ºC for 1h forms a mixture of oxide layers of Al_2O_3 and TiO_2 oxides,

where the outermost layer is mainly TiO_2. Thermal oxidation of Ti-6Al-4V at temperatures between 500°C and 800°C originates stable layers of titanium oxides, mainly rutile and anatase (30). García-Alonso *et al.* (12) found that thermal oxidation of Ti-6Al-4V at 500°C for 1h originates a rutile scale in which Al_2O_3 nuclei begin to appear. They observed that at 700°C for 1h, the proportion of Al_2O_3 nuclei was higher than that observed at 500°C. Guleryuz and Cimenoglu (14) determined that the surface oxide formed on thermally oxidized Ti-6Al-4V surfaces (at 600°C for 60h) was mainly rutile with some amounts of anatase, while thermal oxidation at 650 °C for 60h originated a layer of rutile on Ti-6Al-4V.

The corrosion behavior of the thermally oxidized gamma-TiAl alloy Ti-48Al-2Cr-2Nb (at. %) was studied *in vitro* using Ringer's solution (4,30). By means of potentiodynamic polarization and electrochemical impedance spectroscopy (EIS) it was found that thermal oxidation (autoclaved at 121°C and 15 psi, in air at 500°C or 800°C, each of 1 h) rendered the Ti-48Al-2Cr-2Nb material extremely corrosion resistant. The titanium alloy used for comparison (Ti-6Al-4V) showed similar results. Electron backscattering using SEM showed the formation of an oxide layer on gamma-TiAl with a thickness of about 1 μm as a result of the autoclaving process. Thickness of the oxide layer on gamma-TiAl oxidized at 500ºC and 800ºC were approximately 1 μm and 2-3 μm, respectively. The formation of a 1-2 μm oxide layer on Ti-6Al-4V samples, autoclaved and oxidized at 500ºC was observed, while a thicker porous layer (~10 μm) resulted on samples oxidized at 800ºC. The gamma-TiAl alloy oxidized at 500ºC showed the best corrosion resistance possibly because of the formation of a passive and highly corrosion resistant Al_2O_3 layer as indicated by X-ray diffraction analyses (XRD). The gamma-TiAl samples oxidized at 800ºC showed a lower corrosion resistance possibly due to the formation of a more porous mixed titanium oxide/ alumina layer. The results of XRD patterns for Ti-6Al-4V samples treated at 500ºC revealed the presence of the titanium oxide Ti_6O, while the samples treated at 800ºC contained mainly two allotropic modifications of the titanium oxide (TiO_2), which are rutile and anatase (30).

Scientists have reported the effect of thermal oxidation treatments of cp-Ti and Ti-6Al-4V on osteoblastic behavior *in vitro* (9,11,12,52-54). Bess *et al.* (52) compared the adhesion of human embryonic palatal mesenchymal cells (HEPM cell line) on both non heat-treated and heat-treated (750ºC, 90 min) titanium samples at different time points (0, 3, 6, and 9 days) using the hexosaminidase assay. The amount of HEPM cells attached on heat-treated surfaces was

significantly greater compared to non heat-treated surfaces at all time points tested. In addition, they found higher alkaline phosphatase (ALP) specific activity, and higher matrix associated protein synthesis on cells cultured on heat-treated Ti surfaces compared to non heat-treated Ti surfaces. Using an XRD assay, they determined that the oxide layer formed on heat-treated surfaces was crystalline rutile (TiO_2), whereas the non oxidized samples were covered by an amorphous layer of titanium oxide (52).

Feng *et al.* (53) assessed the effect of different thermal oxidation modalities (600ºC for 30 min in air, oxygen or water vapor) of cp-Ti disks on the adhesion of primary cultures of rabbit osteoblasts after 24h of incubation. They found that cell adhesion and alkaline phosphatase specific activity were greater on heat treated samples compared to control surfaces (non heat-treated). However, the amount of cells attached on the disks oxidized in oxygen and air at 600ºC for 30 min was higher compared to disks oxidized at 600ºC for 30 min in water vapor, which were the roughest surfaces. They hypothesized that increased surface energy originated by thermal oxidation on the surface of cp-Ti disks produce more surface active sites (surface hydroxyl groups) and higher reaction potential favoring the cell attachment and proliferation.

Kern *et al.* (54) evaluated protein adsorption and human embryonic palatal mesenchymal cells (HEPM cell line) adhesion on both non heat-treated and heat-treated (750ºC, 90 min) titanium samples, using the bicinchoninic acid protein assay and the hexosaminidase assay, respectively. After 3h of culture, no significant differences in protein adsorption and cell attachment were observed between the two groups. However, they observed that oxidation treatment of Ti resulted in the conversion of amorphous oxide to crystalline anatase.

García-Alonso *et al.* (12) studied the adhesion of primary cultures of human osteoblasts on thermally oxidized (500ºC and 700ºC in air, for 1h) and non oxidized (polished with 1μm diamond paste) Ti-6Al-4V samples at different time points (30 min, 1, 2, and 24h). Polystyrene was used as the control surface. They observed that the number of cells attached on all the implant materials after 30 min, 1 and 2h was significantly greater than attachment on control. However, after a 24h attachment period there was no significant difference in the attachment of osteoblasts on any of the materials as compared to control. In addition, they did not find significant differences between the percentage of attachment on non oxidized samples and the thermal oxidation treatments for each duration. However, the comparison of cell attachment on both thermally oxidized surfaces after 1 and 2h showed enhanced osteoblast adhesion on Ti-6Al-

4V oxidized at 700ºC. McDonald *et al.* (8) evaluated the effect of different thermal and chemical surface treatments (thermal oxidation at 600ºC for 1h in either air or pure oxygen, peroxide treatment, peroxide treated and thermally oxidized samples with butanol posttreatment) of Ti-6Al-4V alloy on the adhesion of MG63 osteoblast cells after 2h of culture, using the hexosaminidase assay. They assessed cell attachment on the different surfaces uncoated and coated with fibronectin 0.1 nM (a concentration of fibronectin that does not induce cell attachment by itself). They found that thermal oxidation in air, and thermal oxidation (in air and in pure oxygen) with butanol posttreatment increased cell attachment when surfaces were pretreated with fibronectin 0.1 nM. On the contrary, they did not find significant differences in cell attachment on the different uncoated samples (8).

Saldaña *et al.* (9) studied the adhesion of primary human osteoblasts on thermally oxidized (500ºC and 700ºC in air, for 1 h) and non oxidized Ti-6Al-4V samples at different times (15 min, 1, 2, 3, and 24 h). The control surface was the polystyrene. They used the dye 2',7'-bis-(2-carboxyethyl)-5-carboxyfluorescein (BCECF), which shifts from a non fluorescent to a fluorescent dye when it is internalized by living cells, to determine the cell attachment on the different surfaces. It was observed that the number of attached cells increased significantly as a function of time until 3h, on all tested surfaces. After 15 min, the number of cells attached on the non oxidized and both oxidized surfaces was greater than the number of cells attached on the control surface. There were significant differences among the amount of cells attached on the surfaces oxidized at 500ºC, at 700ºC, and the non oxidized surfaces. The surface with the higher number of attached cells was that oxidized at 700ºC, whereas the non oxidized surface had a lower number of cells attached. After 1 and 2h, the number of cells attached on the surfaces oxidized at 700ºC was significantly greater than the number of cells attached on both the oxidized at 500ºC and the non oxidized surfaces. After 3h and 24h there were no significant differences in the number of cells attached on the different surfaces. They also evaluated cell attachment on both thermally oxidized (at 500ºC and 700ºC) and non oxidized Ti-6Al-4V surfaces by detecting the expression of integrin β1 and Focal Adhesion Kinase phosphorylated on Y397 (FAK–Y397) by flow cytometry, and the expression of FAK-Y397 by immunofluorescence assays at different times (0.5, 1, 1.5, 2, 3, and 24h). They could not detect any difference in the percentage of cells expressing integrin β1 on the different alloys at 0.5, 1, 2, 3, and 24h. However, they detected an increase in β1 integrin expression on both thermally

oxidized surfaces after 1.5h, as compared with the non oxidized samples. In addition, after 1.5h the number of cells attached on the surfaces oxidized at 700ºC was greater compared to cell attachment on the surfaces oxidized at 500ºC. Similar results were obtained in the detection of FAK-Y397 by flow cytometry and by immunofluorescence assays.

Saldaña *et al.* (11) evaluated the *in vitro* biocompatibility of alumina blasted Ti-6Al-4V thermally oxidized (500ºC, 1h) surfaces. They assessed the cell attachment of human primary osteoblasts cultured for 0.25, 0.5, 1, 2, 3, and 24 h on three types of surfaces: polished Ti-6Al-4V (smooth surface), alumina blasted Ti-6Al-4V and alumina blasted Ti-6Al-4V thermally oxidized (500ºC, 1h). The blasting process originates a rough surface. They found that differences in roughness of oxidized and non oxidized blasted samples were not significant. Using a MTT [3-(4,5-dimethylthiazolyl-2)-2,5-diphenyltetrazolium bromide] assay, they determined that the number of attached cells increased significantly with increasing testing time until 3h, on all tested surfaces. The percentage of cells attached on polished samples (smooth surfaces) was significantly higher than on rough samples (oxidized and non oxidized blasted surfaces) for 0.25 to 3h. However, they found that the number of attached cells on the oxidized blasted specimens was higher than on only blasted specimens for 0.25 to 3h. At 24h, the amount of cells attached on all tested surfaces was similar. They also evaluated the viability and the proliferation of osteoblast cells seeded on polished Ti-6Al-4V, alumina blasted Ti-6Al-4V and alumina blasted Ti-6Al-4V thermally oxidized (500ºC, 1h) surfaces after 3 and 7 days of incubation. Cell viability was assessed using the alamarBlue assay (a redox indicator that changes in color in response to metabolic activity). Cell proliferation was assessed quantifying the DNA cell content using the bisbenzimidazole fluorescent dye Hoechst 33342. They observed that osteoblast proliferation and the number of viable cells increased significantly between days 3 and 7 on all the surfaces. However, they found that there was less cell proliferation and fewer number of viable cells on the alumina blasted surface compared with both the polished and the alumina blasted thermally oxidized surfaces, where the cell attachment and viability were similar (11).

In summary, some previous studies have established that thermal oxidation of Ti and Ti-6Al-4V increases cell attachment and cell differentiation as well as the corrosion resistance of the Ti alloys. Thus, it is expected that thermally oxidized gamma-TiAl surfaces would exhibit similar or better biocompatibility properties compared to autoclaved gamma-TiAl surfaces. Depending on thermal oxidation conditions different surface oxides are formed on Ti alloys; thus,

it is expected that osteoblast cells respond differently to surface oxides formed on thermally oxidized at 500°C and at 800°C gamma-TiAl surfaces.

3 OBJECTIVES

3.1 GENERAL OBJECTIVE

- To determine the effects of thermal oxidation of gamma-TiAl on the *in vitro* adhesion of human fetal osteoblast cells (hFOB 1.19 cell line).

3.2 SPECIFIC OBJECTIVES

- Observe the morphology of the human fetal osteoblast cell line (hFOB 1.19) cultured on glass at different time points (1, 3, 5, 7, 14, 21 and 28 days).

- Evaluate (quantitatively and qualitatively) human fetal osteoblast adhesion on thermally oxidized (500 ºC or 800 ºC in air, 1 h) and autoclaved gamma-TiAl disks.

- Evaluate (quantitatively and qualitatively) human fetal osteoblast adhesion on thermally oxidized (500 ºC or 800 ºC in air, 1 h) and autoclaved Ti-6Al-4V disks.

- Compare the human osteoblast adhesion on gamma-TiAl disks versus adhesion on Ti-6Al-4V disks.

4 MATERIALS AND METHODS

4.1 PREPARATION OF DISKS

The gamma-TiAl used in this study is Ti-48Al-2Cr-2Nb (at. %). Gamma-TiAl rods of both 5 and 9 mm in diameter were machined using electric discharge machining (EDM) from as-received rods of 25 mm diameter. Gamma-TiAl disks of both 5 and 9 mm in diameter and an approximate thickness of 1 mm were manually cut from the respective machined rods, using a low speed saw (Buehler™). Their surfaces were prepared manually in an Ecomet 3 (Buehler™) by wet grinding with 240, 320, 400 and 600 grit silicon carbide paper to generate a rough surface. These metal disks were ultrasonically cleaned in 0.8% Alconox (Fisher, Pittsburgh, Pennsylvania) and 95% ethanol for 10 min each, while rinsing with deonized water between each application. The metal disks were dried and then oxidized in a laboratory furnace (CM Furnaces Inc., Bloomfield, NJ) in air at 500°C (GTi5) or at 800°C (GTi8) for 1h. They were transported aseptically to the cell culture laboratory and placed in 48-well cell culture plates (Corning, Corning, New York). Gamma-TiAl disks (GTi) polished and cleaned as described previously, and subsequently sterilized by autoclaving (121ºC, 15 psi, 15 min) were used as controls. Ti-6Al-4V alloy disks, 5 mm or 9 mm in diameter and 1 mm in thickness approximately, manually cut from machined wrought ($\alpha+\beta$) annealed rods and oxidized at 500°C (TiV5) or 800°C (TiV8) and sterilized by autoclaving (TiV), were processed as described for gamma-TiAl disks and used for comparison purposes.

4.2 CELL LINE

Human osteoblast cell line hFOB 1.19 (CRL-11372) (ATCC, Manassas, Virginia) were cultured in 90% Dulbecco's Modified Eagle's Medium Nutrient Mixture F-12 Ham (DMEM) (Sigma-Aldrich, St. Louis, Missouri) with 2.5 mM L-Glutamine and 15mM Hepes, without phenol red, supplemented with 0.3 mg/mL G-418 (Calbiochem, San Diego, California) and 10% Fetal Bovine Serum (FBS) (Hyclone, Logan, Utah). Cells were grown in 25 cm^2 plastic culture flasks (Corning, Corning, New York) and incubated at 33.5 ºC until confluence. At approximately 100% confluence, cells were washed three times with phosphate buffered saline (PBS) (137mM NaCl, 2.7mM KCl, 4.3mM Na_2HPO_4, 1.4mM KH_2HPO_4) and harvested using

0.25% trypsin- 0.53mM EDTA (Gibco, Gaithersburg, Maryland) at 37°C for 5 min. Cells were pelleted by low-speed centrifugation (3,300 rpm) for 5 minutes, and subcultured in a 1:3 ratio

4.3 HEXOSAMINIDASE ASSAY

Cells were seeded in 48-well plates (Becton Dickinson, Lincoln Park, NJ) at a density of 5×10^4 cells/cm^2 on GTi, GTi5, GTi8, TiV, TiV5 and TiV8 disks (5 mm in diameter), involving 9 total disks per treatment. Cells cultured on polystyrene were used as cell growth control. Samples were incubated for 24h (hereafter referred to 1 day), 7 or 14 days in serum containing media. The samples incubated for 1 and 7 days were incubated at 33.5ºC, and the samples incubated for 14 days were initially incubated at 33.5ºC for 7 days, and subsequently at 39.5ºC for 7 days to allow cell differentiation. After incubation the samples were gently rinsed three times in PBS to remove the unattached cells and the disks were transferred from the 48-well tissue culture plate to a 96-well plate (Becton Dickinson, Lincoln Park, NJ). The number of attached cells was quantified using the hexosaminidase assay (8,52,55,56). 7.5 mM p-nitrophenyl-N-acetyl-β-D-glucosaminide (hexosaminidase substrate) in 0.1M citrate buffer (pH 5.0) was mixed with an equal volume of 0.5 % Triton X-100 in water, and 60 μL of the resultant solution added per cell culture well. The 96-well culture plate was incubated for 1h at 37°C. The reaction was stopped by the addition of 90 μL of 50 mM glycine buffer (pH 10.4), containing 5 mM EDTA. The reagents of the β-N-Acetylglucosaminidase Assay Kit (CS0780, Sigma, St. Louis, MO) were used for the hexosaminidase assay. The disks were carefully removed from the 96-well culture plate leaving the solution in the wells. The absorbance of the remaining solution was measured at a wavelength of 405 nm using a microplate reader (ThermoMax, Molecular Devices). A standard curve of hexosaminidase activity versus cell number measured by a Neubauer chamber was run for each experiment (Appendix A). All of the measurements of cell number in the experimental ("unknown") wells were based on hexosaminidase activity and extrapolation from the standard curve.

Human fetal osteoblasts of the cell line hFOB 1.19, ranging from 500 to 55000 viable cells per well, were seeded in 96-well plates and incubated for 24h at 39.5°C to run each standard curve. Cell counting was performed on a hemocytometer using the vital dye trypan blue. Osteoblasts cells used for a standard curve were obtained from the same cell suspension

employed to seed on the different disks used in the corresponding experiment. After incubation, cells were assayed by the hexosaminidase assay. Wells containing a mixture of the hexosaminidase substrate with 0.5% Triton X-100 and 50 mM glycine buffer (pH 10.4), but without cells, were used as the microplate reader blank.

4.4 SCANNING ELECTRON MICROSCOPY (SEM) ANALYSIS

Cell adhesion on the different surfaces was evaluated qualitatively by SEM. Cells were seeded in 48-well plates (Becton Dickinson, Lincoln Park, NJ) at a density of 5 x 10^4 cells/cm^2 on GTi, GTi5, GTi8, TiV, TiV5 and TiV8 disks (9 mm in diameter). Samples were incubated for 7 days at 33.5ºC, and then for 7 days at 39.5ºC allowing osteoblast differentiation. GTi, GTi5, GTi8, TiV, TiV5 and TiV8 disks incubated with culture media but without cells were used as negative controls. Cells growing on glass coverslips were used as cell growth controls. After the incubation period, samples were washed carefully with PBS and fixed overnight in 4% glutaraldehyde buffered in PBS at 4ºC. After washing three times with PBS, the samples were dehydrated in graded alcohol ranging from 10% to 100% ethanol for 10 min each. The 100% ethanol solution was changed three times every 10 min. After critical point drying (EMS 850) (Electron Microscopic Science, Washington) samples were mounted on stubs and were sputtered coated with gold and palladium in EMS 550X (Electron Microscopic Science, Washington). Samples were then examined with a JEOL JSM-5410 LV SEM (JEOL, Japan) at 10 or 15 KV using variable magnification (75, 150, 500, 1500 and 5000X). Two independent experiments, with each experiment performed in triplicate were carried out.

4.5 TIMECOURSE MORPHOLOGICAL CHARACTERIZATION OF THE CELL LINE hFOB 1.19 BY SEM

Cells were seeded on acid washed glass coverslips at a density of 5 x 10^4 cells/cm^2 and incubated for 1 (24 h), 3, 5, and 7 days at 33.5ºC, and subsequently at 39.5ºC for 14, 21 and 28 days. After incubation, the samples were processed as was described for SEM. Samples were examined with a JEOL JSM-5410 LV SEM (JEOL, Japan) at 10 or 15 KV using variable magnification (75, 150, 500, 1500 and 5000X). Three independent experiments were performed, with each experiment performed in duplicate.

To acid wash the glass coverslips, they were immersed in 1M HCl and heated at 50-60ºC for 4h. After cooling, the HCl solution was discarded and coverslips were washed thoroughly with distilled water. They were ultrasonically cleaned in deonized water for 20 min. Finally, they were ultrasonically cleaned in 50%, 70%, and 95% ethanol for 10 min each. The coverslips were stored in 95% ethanol at 4ºC until used.

4.6 IMMUNOFLUORESCENT LABELING

In order to evaluate osteoblast adhesion qualitatively on autoclaved and thermally oxidized gamma-TiAl and Ti-6Al-4V disks, β1 integrin and vinculin, which are components of focal adhesions, were immunostained in hFOB 1.19 cells seeded on the different surfaces. Cells were seeded in 48-well plates (Becton Dickinson, Lincoln Park, NJ) at a density of approximately 1.5 x 10^4 cells/cm^2, as determined by a hemocytometer count, on GTi, GTi5, GTi8, TiV, TiV5 and TiV8 disks of 9 mm in diameter. Samples were incubated for 3 days at 33.5ºC, and then for 4 days at 39.5ºC allowing osteoblast differentiation. After incubation, the cells were fixed using 3.7% formaldehyde in 1x PBS at room temperature for 10 min and washed twice with 1x PBS. Cells were permeabilized and non-specific staining was blocked by incubation in blocking solution [0.1% BSA, 0.05% saponin, 5% normal goat serum (NGS) in 1x PBS] for 1h at room temperature. The blocking solution was removed and the expression of β1 integrin and vinculin in the cells cultured on the different surfaces was simultaneously detected by incubation with 75µL of a mixture of mouse anti-human β1 integrin monoclonal antibody (1:100 v/v) (MAB1987Z, Chemicon, Temecula, CA) and rabbit anti-human vinculin polyclonal antibody (1:50 v/v) (SC-5573, Santa Cruz Biotechnology, Santa Cruz, CA), respectively. After 2h of incubation at room temperature with shaking (80 rpm) samples were washed three times with a solution of 0.1% BSA and 0.05% saponin in 1x PBS for 5 min each and followed by the addition of 75 µL of a mixture of secondary antibodies diluted 1:100 (v/v) in blocking solution per well. Alexa Fluor ® 647 goat anti-mouse IgG (H+L) (A21236, Molecular Probes, Eugene, OR) and goat anti-rabbit IgG (H+L) Rhodamine conjugated secondary antibody (AP307R, Chemicon, Temecula, CA) were used as secondary antibodies. After 1 hour of incubation at room temperature with shaking (80 rpm) in the dark, the samples were washed with 1x PBS three times for 10 min each. Cell nuclei were contrast-labeled in blue by incubation for 5 min

with 0.5μg/ml DAPI (4',6-Diamidino-2-phenylindole hydrochloride) (D9542, Sigma-Aldrich, Saint Louis, MO), mounted in 24 x 60 mm coverslips with ProLong™ Gold antifade reagent (Invitrogen, Eugene, Oregon) and stored at 4ºC in the dark. Samples were observed using an inverted confocal laser scanning microscope (FluoView™ 300, Olympus, USA) equipped with 405LD, 543 Green HeNe, and 633 Red HeNe lasers, and a 60x/1.4 oil immersion objective.

GTi, GTi5, GTi8, TiV, TiV5 and TiV8 disks, where hFOB 1.19 cells were seeded and incubated as described previously, but where the primary and secondary antibodies were replaced with blocking solution, were used as controls for both metal and cellular autofluorescence. Since preliminary experiments indicated that gamma-TiAl and Ti-6Al-4V exhibit autofluorescence at the wavelength of emission of Alexa Fluor ® 647 (668 nm) and hFOB 1.19 cells at the wavelength of emission of Rhodamine (573 nm), both metal and cellular autofluorescence were measured on the same set of samples at 668 nm and 573 nm, respectively. Cells growing on glass coverslips were used for positive, negative, isotype, and primary and secondary antibody controls. The positive control samples were incubated with the two primary and secondary antibodies as described previously for the experimental samples. Coverslips where both the primary and secondary antibodies were omitted were used as negative controls. For isotype controls, the primary antisera were replaced with non-immune mouse or rabbit serum, respectively. For primary antibody control, the secondary antibodies were replaced with blocking solution, and for secondary antibody control, the primary antibodies were replaced with blocking solution.

The average fluorescence intensity (in arbitrary units on a scale from 0 to 255 units) of Alexa Fluor ® 647 and Rhodamine in an area of 7.8464 x 10^5 μm^2 was measured for the experimental samples (cells seeded on GTi, GTi5, GTi8, TiV, TiV5 and TiV8 disks), and for the autofluorescence controls (metal and cellular autofluorescence) using the software Fluoview version 4.3, Olympus Corporation. The fluorescence intensity determinations were made at a distance of 1μm from the substrate surfaces. This focal depth was chosen to avoid or reduce the metal autofluorescence. Red HeNe laser with an intensity of 50%, PMT = 544V, Gain = 4.5X and offset = 1.0% were the settings of the confocal microscope used to measure the fluorescence intensity of Alexa Fluor ® 647 (β1 integrin) whereas Green HeNe laser with an intensity of 50%, PMT = 724V, Gain = 4.5X and offset = 5.0% were the settings to measure the fluorescence intensity of Rhodamine (vinculin). Pinhole 2 was used for all the measurements. The metal and

cellular autofluorescence were subtracted from the fluorescence of each sample using Fluoview software version 4.3. The immunofluorescent detection of β1 integrin and vinculin was performed in duplicate.

4.7 STATISTICAL ANALYSIS

The hexosaminidase assay was performed on three independent experiments, each with three replicates, for a total of nine replicates per surface evaluated (GTi, GTi5, GTi8, TiV, TiV5, and TiV8) for each time period of culture (1, 7 and 14 days). The data of the hexosaminidase assay is presented in Appendix B as mean ± standard deviation (S.D.) of the number of attached cells on the different surfaces for each time period. Each value represents the mean of the measurements (using three disks) of cell attachment performed on a specific surface tested in one of the three independent experiments. After testing that the variances of the three experiments were homogeneous (Levene's test, $p \geq 0.05$), a factorial analysis of variance (ANOVA) was used to assess the main effect and the significant interactions between type of metal (gamma Ti-Al or Ti-6Al-4V), incubation period (1, 7, or 14 days), and temperature of oxidation (autoclaving [121°C], thermal oxidation at 500°C or 800°C). All factors were considered fixed. When these interactions were found, they were graphically analyzed. In addition, multiple contrasts of hypotheses were performed, using 95% Bonferroni intervals of confidence to control the experimentwise error rate. When no interactions were found, an ANOVA was performed, followed by the Tukey multiple comparison test, analyzed by 95% confidence intervals, in order to check for the presence of significant differences in cell attachment on the surfaces tested. The *p* values ≤0.05 were considered to be statistically significant. All analyses were performed using Minitab® 14 (Minitab Inc).

5 RESULTS

5.1 VISUAL APPEARANCE OF AUTOCLAVED AND THERMALLY OXIDIZED DISKS

The macroscopical appearance of autoclaved and thermally oxidized gamma-TiAl and Ti-6Al-4V disks is shown in Figure 1.

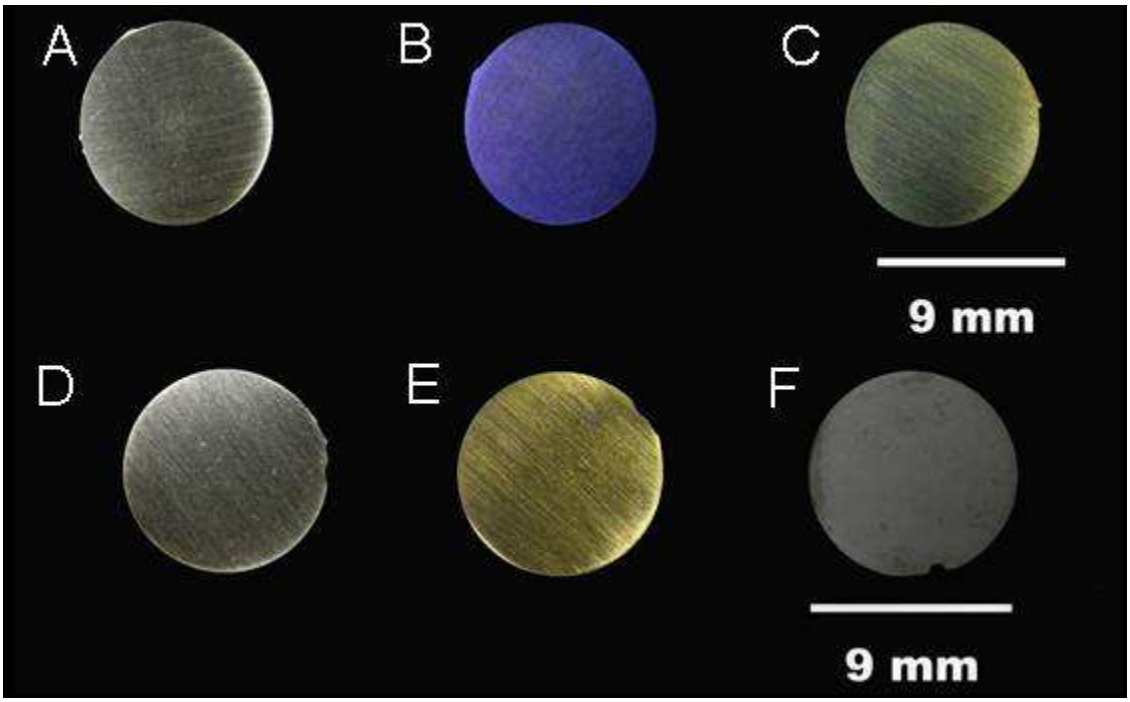

Figure 1. Visual appearance of autoclaved (A,D), thermally oxidized at 500°C (B,E) and at 800°C (C,F) gamma-TiAl and Ti-6Al-4V disks, respectively.

The autoclaved gamma TiAl and Ti-6Al-4V surfaces appeared gray metallic. The surface of the gamma-TiAl disk oxidized at 500°C was blue colored whereas the surface of the Ti-6Al-4V disk oxidized at the same temperature was dark yellow. The surface of the gamma-TiAl disk oxidized at 800°C appeared light yellow (golden appearance) whereas the Ti-6Al-4V disk oxidized at the same temperature appeared dark gray. Parallel grooves, originated by the wet grinding, were observed on all the surfaces, except on the Ti-6Al-4V surface oxidized at 800°C (Fig. 1F)

5.2 HEXOSAMINIDASE ASSAY

The average number and standard deviation (S.D.) of osteoblast cells attached on the different surfaces at each time point are shown in Figure 2. The interaction between type of metal (gamma-TiAl or Ti-6Al-4V), incubation period (1, 7, or 14 days) and the temperature of oxidation (121, 500, or 800°C) was significant ($p \leq 0.05$, Appendix C1; Fig.3). There were no significant differences in cell attachment among the six surfaces studied after 24 h (hereafter referred as 1 day) of incubation (Appendix D1). In contrast, the number of osteoblast cells attached to TiV8 surfaces was significantly less compared to the other surfaces tested at both 7 and 14 days post-incubation (Appendixes D2 and D3, respectively; and Fig. 2). Additionally, cell number was reduced over time on TiV8 (Fig. 2).

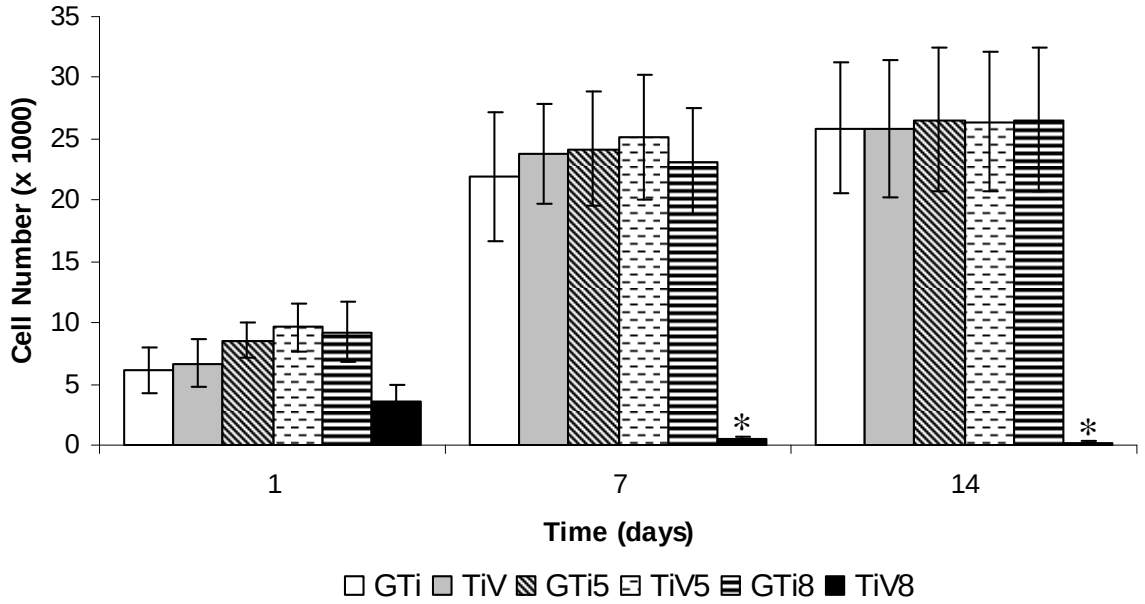

Figure 2. Human osteoblast (hFOB 1.19) cell attachment on autoclaved and thermally oxidized at 500°C and 800°C gamma TiAl and Ti-6Al-4V disks. Cells were cultured on GTi, GTi5, GTi8, TiV, TiV5, and TiV8 surfaces for 1, 7, and 14 days. The data are expressed as the number of attached cells on the different substrates determined by the hexosaminidase assay. Each value represents the mean ± S.D. of three independent experiments, each performed in triplicate (N=9). *$p \leq 0.05$ compared to all other surfaces tested, at the corresponding time point.

The factorial ANOVA carried out excluding the data of cell attachment on GTi8 and TiV8 (thermally oxidized at 800°C gamma-TiAl and Ti-6Al-4V surfaces, respectively) showed that the interaction between the three factors (type of metal, time of incubation and temperature of oxidation) yielded no significant differences ($p \geq 0.05$, Appendix C2). In addition, there were

no significant differences in cell attachment among the four surfaces studied at the three time points tested (1, 7, and 14 days). Cell attachment increased significantly between days 1 and 7 on all tested surfaces ($p \leq 0.05$). After this time, the number of attached cells remained constant on all assessed surfaces (Fig. 4, Appendix C3).

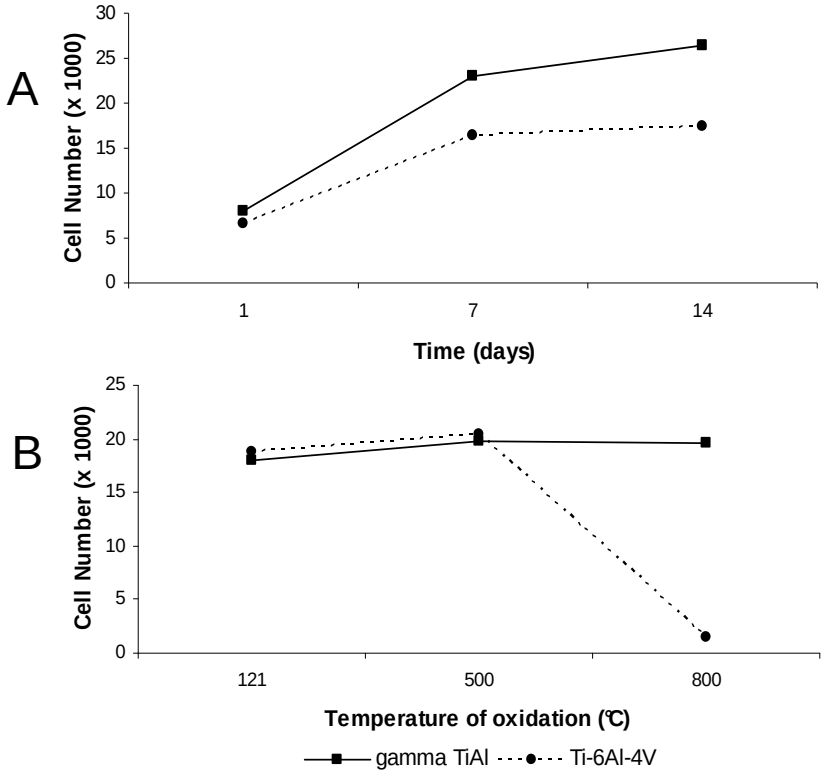

Figure 3. Interaction plot for number of cells attached on gamma-TiAl and Ti-6Al-4V disks versus time of incubation (A) and temperature of oxidation (B). The ANOVA demonstrates that the interaction among type of metal (gamma-TiAl or Ti-6Al-4V) and time (1, 7, or 14 days) is significant ($p \leq 0.05$) as well as the interaction among type of metal (gamma-TiAl or Ti-6Al-4V) and temperature of oxidation (121°C, 500°C, or 800°C).

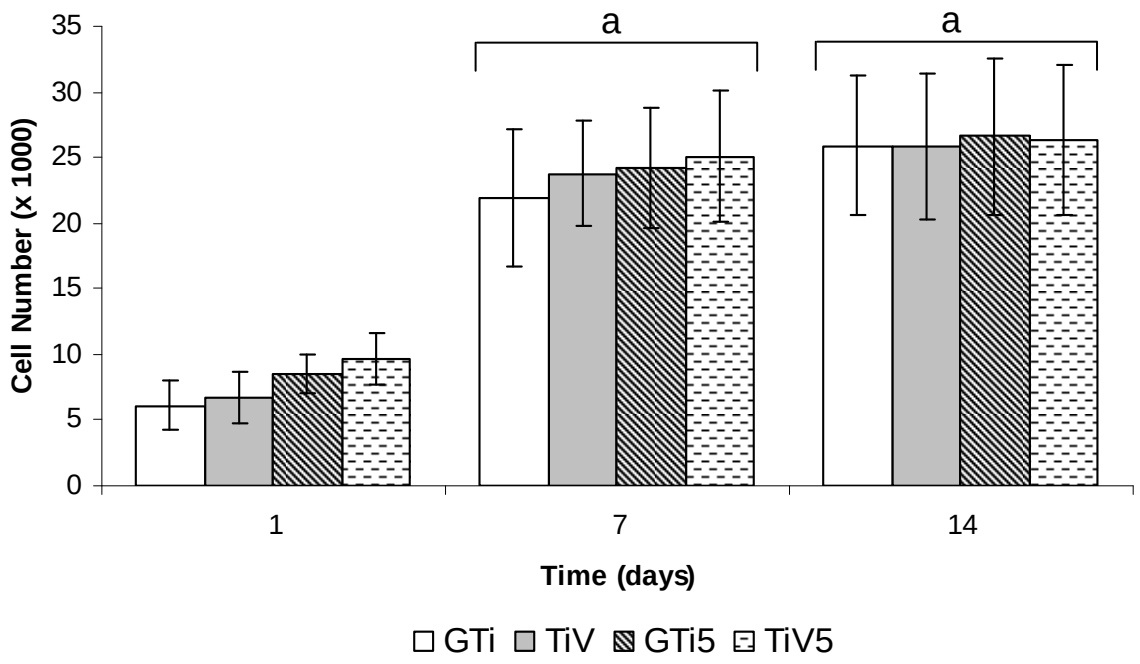

Figure 4. Human osteoblast (hFOB 1.19) cell attachment on autoclaved and thermally oxidized at 500°C gamma TiAl and Ti-6Al-4V disks. Cells were cultured on GTi, GTi5, TiV, and TiV5 surfaces for 1, 7, and 14 days. The data are expressed as the number of attached cells on the different substrates determined by the hexosaminidase assay. Each value represents the mean ± S.D. of three independent experiments, each performed in triplicate (N=9). $^{a}p \leq 0.05$ compared to day 1.

5.3 TIMECOURSE MORPHOLOGICAL CHARACTERIZATION OF THE CELL LINE hFOB 1.19 BY SEM

After 24h (1 day) of incubation, the osteoblasts had spread and flattened on the glass surfaces (Figures 5A-C). The cells grew as discontinuous (not confluent) monolayers of mainly elongated and flattened cells, although some cells showed variable appearance (spherical, oval or polygonal). The osteoblasts looked scattered in all directions and they did not have a regular orientation (Fig. 5A). Some of the spherical cells (approximately 15μm in diameter, white arrowheads Figs. 5B and 5C) grew over the elongated cells (70-100μm long and 5-10μm wide approximately). The spherical cell displayed in Figure 5C had a rough surface but lacked cell projections. After a 3 day incubation period, the cell density increased although the monolayer was not confluent. The majority of osteoblasts still remained with a flattened and elongated shape (white arrow, Fig. 5F). However, some polygonal and spherical cells were also seen at this time point. Numerous thin filopodia (slender cytoplasmic projections) extending from the cells in

all directions, and allowing cell-substrate and cell-cell interactions, were observed (asterisk, Figs. 5E and 5F). In addition, they displayed broad lamellipodia (sheet-like cytoplasmic protrusions) (black stars, Figs. 5E and 5F). Cell density was increased and started to form a continuous monolayer by day 5 of culture. The bulk of the cells still remained with an elongated shape (white arrows, Figs. 5G and 5H) but some polygonal, spherical and oval cells (white arrowhead, Fig. 5H) were also present. Osteoblasts cultured for 5 days displayed numerous thin filopodia (asterisk, Fig. 5I) and appeared to be thicker than cells incubated up to 3 days. The cells did not have regular orientation and in some regions started to form a multilayer. A closer view of an oval cell, which was 30μm in length and 20μm in width approximately, is displayed in Figure 5I. This cell, located in a lacuna-like space, showed a ruffled or "blebby" surface (black arrowheads, Fig. 5I) with many thin, capillary-like filopodia extending from the cell body in all directions. After 7 days, a confluent multilayer of cells was observed (Figs. 5J-K). Cellular boundaries were difficult to establish due to the close contact between neighboring cells (Fig. 5J). The multilayer was constituted by elongated and polygonal cells with some round shaped cells (white arrowheads, Figs. 5J and 5K). The rounded cell showed in Figure 5L, which was approximately 18-20 μm in diameter, exhibited a ruffled surface and many filopodia in multiple directions. This cell was in close contact with the underlying cell layer and substratum through filopodia (asterisks, Fig. 5L). The presence of a few small rounded structures which may correspond to mineral nodules (black arrows, Fig. 5K) was noticed. By day 14, a slight decrease in the cell density (Fig. 5M) and the formation of a more stratified multilayer (arrowheads, Fig. 5N) were observed. The osteoblasts remained elongated and polygonal in shape and were parallely oriented. They exhibited such close contact with each other that detection of the complete cellular boundaries was difficult (Fig. 5M). Fibrous networks, which may correspond to fibrillar collagen, were associated with cells (ovals, Figs. 5N and 5O). In addition, there was an increase in the number and size of the nodules of mineralization with a sponge-like morphology (black arrows, Figs. 5N and 5O). After 21 days of incubation the cells maintained the elongated and polygonal shapes but at this time point they did not have a particular orientation. Fibrous networks intimately associated with the cells were also appreciated at this time point (oval, Fig. 5Q). Cellular boundaries were difficult to establish due to close cell-cell and cell-ECM contacts. In addition, there were nodules of mineralization scattered through the samples (black arrows, Figs. 5P and 5Q). At high magnification the mineral nodule shown in Figure 5R (black arrow)

was in close contact with cells and had the sponge-like appearance mentioned previously. At day 28, cell morphological aspects remained constant. Most cells had elongated and polygonal morphologies (white arrow, Fig. 5S), but a few rounded cells were also present (white arrowheads, Figs. 5S and 5T). The rounded cell displayed in Figure 5U had less filopodia than the rounded cells seen at days 5 and 7 although they were similar in size and also showed a ruffled surface. The ECM was more fibrillar at this time point (ovals, Fig. 5U). Many nodules of mineralization intimately associated with the fibrillar network were observed (black arrows, Figs. 5S and 5T).

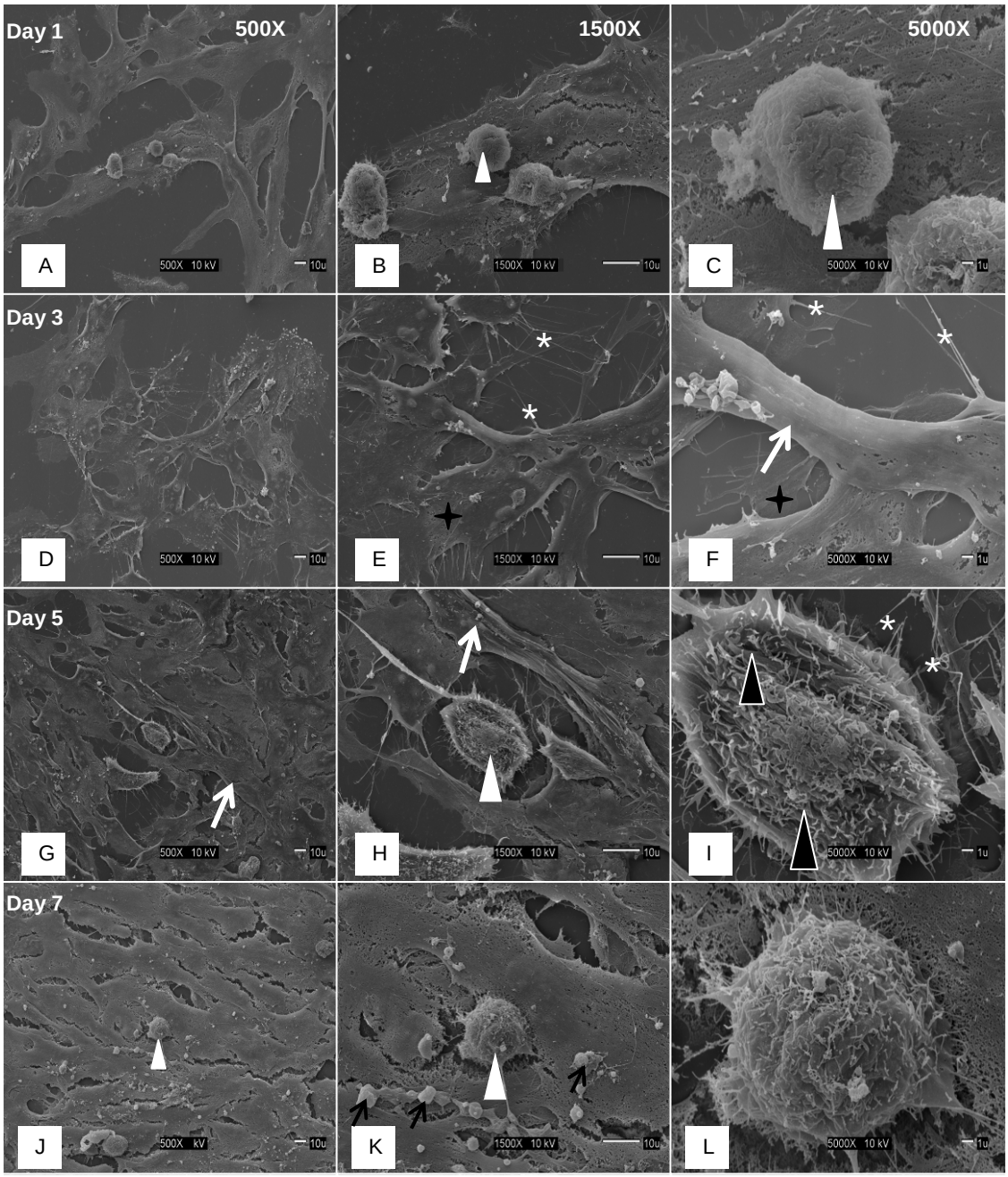

Figure 5. Morphological characterization of the human fetal osteoblast cell line 1.19 (hFOB 1.19 cell line) by SEM. The osteoblasts were seeded on acid washed glass coverslips at a density of 5 x 10^4 cells/cm^2 and incubated for 1 (A-C), 3 (D-F), 5 (G-I), 7 (J-L), 14 (M-O), 21 (P-R), and 28 days (S-U). Each row shows the cell appearance by SEM at each time point at three magnifications (500, 1500, and 5000X), respectively. White arrowheads show spherical or oval cells, asterisks show filopodia, black stars show lamellipodia, white arrows show elongated cells, black arrowheads show ruffled cell surface, black arrows show nodules of mineralization and ovals show fibrous networks. (Scale bar: left and center 10µm, right 1µm).

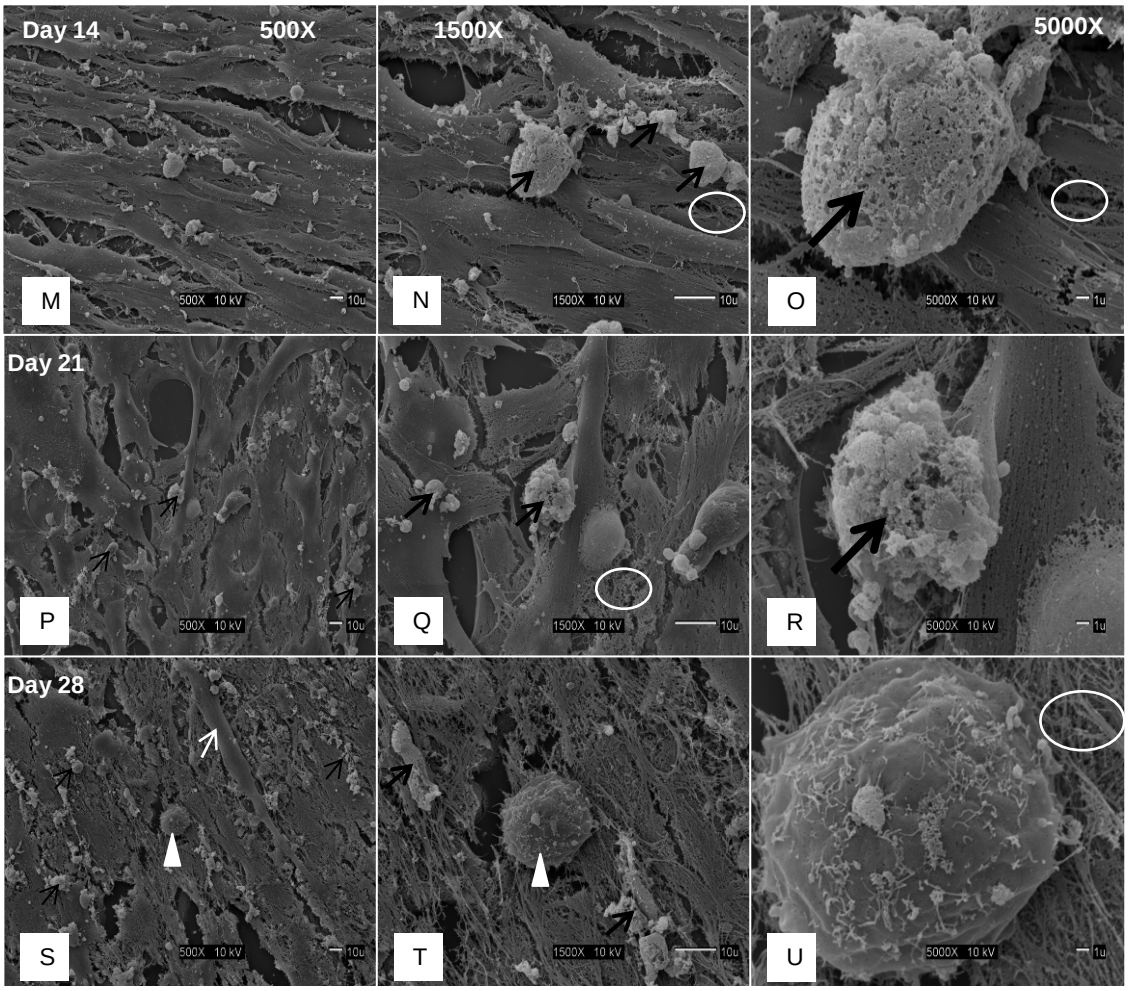

Figure 5, continuation. Morphological characterization of the human fetal osteoblast cell line 1.19 (hFOB 1.19 cell line) by SEM. The osteoblasts were seeded on acid washed glass coverslips at a density of 5 x 10^4 cells/cm^2 and incubated for 1 (A-C), 3 (D-F), 5 (G-I), 7 (J-L), 14 (M-O), 21 (P-R), and 28 days (S-U). Each row shows the cell appearance by SEM at each time point at three magnifications (500, 1500, and 5000X), respectively. White arrowheads show spherical or oval cells, asterisks show filopodia, black stars show lamellipodia, white arrows show elongated cells, black arrowheads show ruffled cell surface, black arrows show nodules of mineralization and ovals show fibrous networks. (Scale bar: left and center 10μm, right 1μm).

5.4 SCANNING ELECTRON MICROSCOPY (SEM) ANALYSIS

Figure 6 shows the appearance of the different surfaces tested before cell seeding. The surfaces of the gamma-TiAl and Ti-6Al-4V samples polished but not autoclaved (Figs. 6A [GTi-P] and 6B [TiV-P], respectively) and polished and autoclaved (Figs. 6C [GTi] and 6D [TiV], respectively) look very similar, exhibiting the polishing marks (parallel grooves and striations). The surface oxide layer present on GTi5 and TiV5 samples (Figures 6E and 6F, respectively) is characterized by the presence of surface scales different in size. On the contrary, the oxide layer present on GTi8 and TiV8 disks is very granular, resulting in a rough surface (Figs. 6G and 6H, respectively). Nevertheless, the oxide granules formed on TiV8 (Fig. 6H) are bigger compared to the granules formed on GTi8 (Fig. 6G), conferring a rougher appearance to the TiV8 surface compared to that of GTi8.

The appearance of the negative control disks, which were incubated with culture media for 14 days (7 days at 33.5ºC and subsequently 7 days at 39.5ºC) but without cells, is presented in Figure 7. The GTi, GTi5, TiV and TiV5 surfaces showed small irregular to rounded surface structures (Fig. 7, white arrows) that resembled the scales observed on GTi5 and TiV5 samples not incubated with culture media (Fig. 6, black arrows). However, these structures were more abundant and irregular in shape and size after incubation with culture media but without cells. There were no apparent differences between the appearance of the GTi8 and TiV8 surfaces previous to and after incubation with culture media (Figs. 6G-6H, and 7C-7F, respectively).

When cells were seeded on disks, SEM images showed that after 14 days of incubation (7 days at 33.5ºC and subsequently 7 days at 39.5ºC) hFOB 1.19 cells were attached on glass coverslips (positive control) as well as on GTi, GTi5, GTi8, TiV and TiV5 disks, but they did not adhere to TiV8 disks (Figs. 8 and 9). The osteoblast cells formed confluent cultures on all the surfaces, except on TiV8. Higher magnification showed that the confluent cultures were multilayered (contained various cell layers) (black arrowheads, Figs. 8E and 9E).

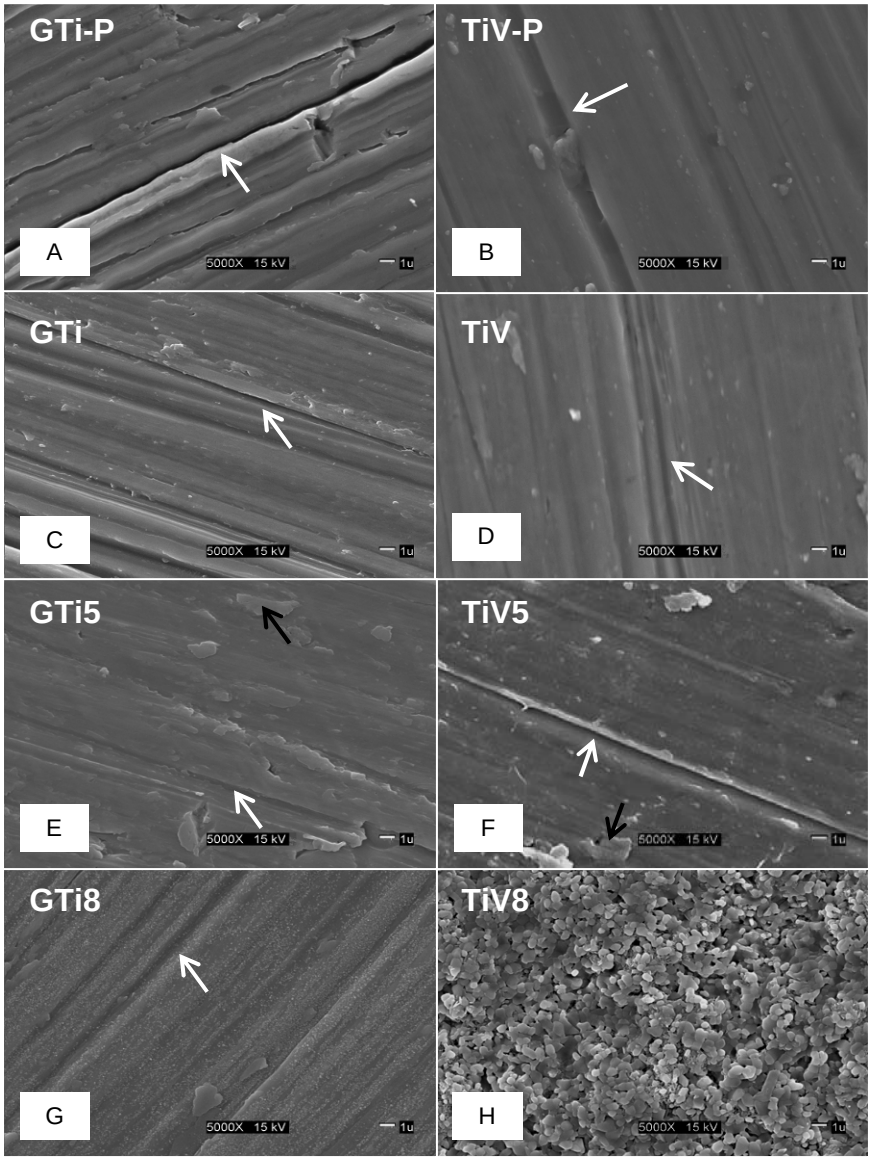

Figure 6. SEM appearance of gamma-TiAl and Ti-6Al-4V disks submitted to different surface treatments but no incubated with culture medium. SEM appearance of a gamma-TiAl disk polished (GTi-P) [A], polished and autoclaved (GTi) [C], thermally oxidized at 500°C (GTi5) [E], and oxidized at 800°C (GTi8) [G]. The SEM appearance of Ti-6Al-4V polished (TiV-P) [B], polished and autoclaved (TiV) [D], thermally oxidized at 500°C (TiV5) [F], and oxidized at 800°C (TiV8) [H] are also showed. Scale bar = 1 µm. White arrows show the polishing marks; black arrows show some oxide scales.

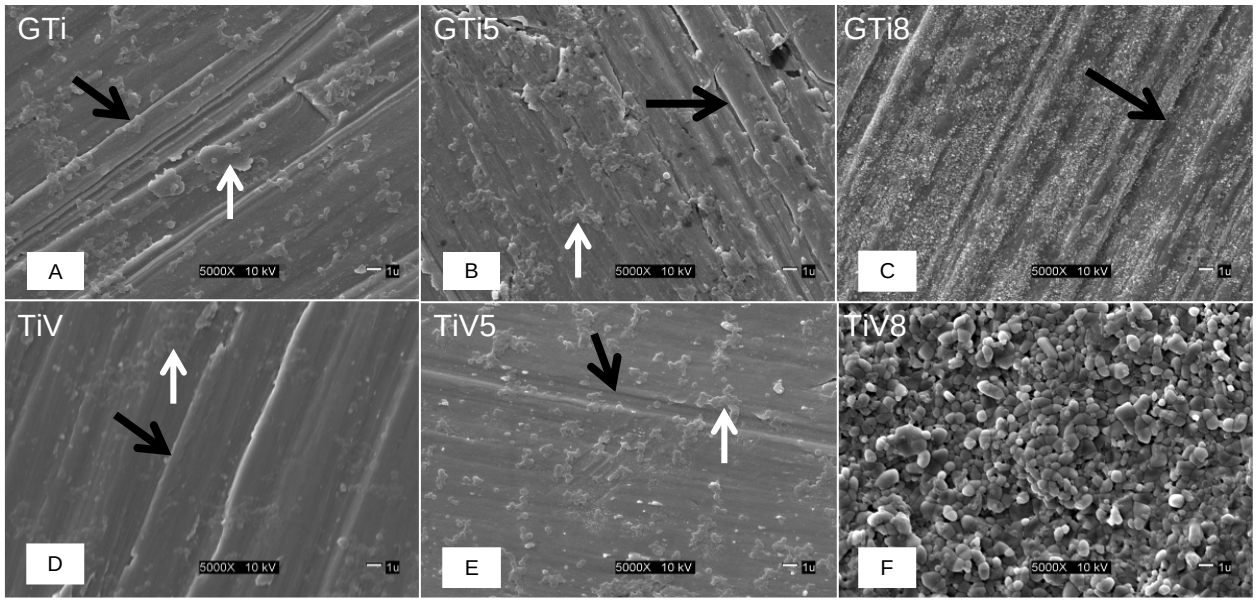

Figure 7. SEM micrographs of the negative control disks (incubated with culture media for 14 days but without cells). GTi (A), GTi5 (B), GTi8 (C), TiV (D), TiV5 (E), and TiV8 (F). Scale bar = 1 µm. Black arrows show the polishing marks; white arrows show precipitates.

No morphological differences of hFOB 1.19 cells grown for 14 days on glass coverslips (positive control), GTi, GTi5, GTi8, TiV and TiV5 surfaces were observed. Cells were mainly elongated, although some cells showed variable appearance (spherical, oval or polygonal) with many filopodia protruding from the cells in all directions (white arrows, Figs. 8I and 9C). Some cells exhibited numerous small sphere-like surface evaginations (black arrow, Fig. 8I). Fibrous networks were present on all the surfaces tested, except on TiV8. These networks were irregularly arranged and were in close contact with the cells (asterisks, Fig. 8I and 9C). Rounded sponge-like structures of different sizes were also observed around the cells on all the surfaces tested, except on TiV8 (white arrowheads, Figs. 8F, and 9F). On the TiV8 samples only small irregular structures were observed (oval, Fig. 9I).

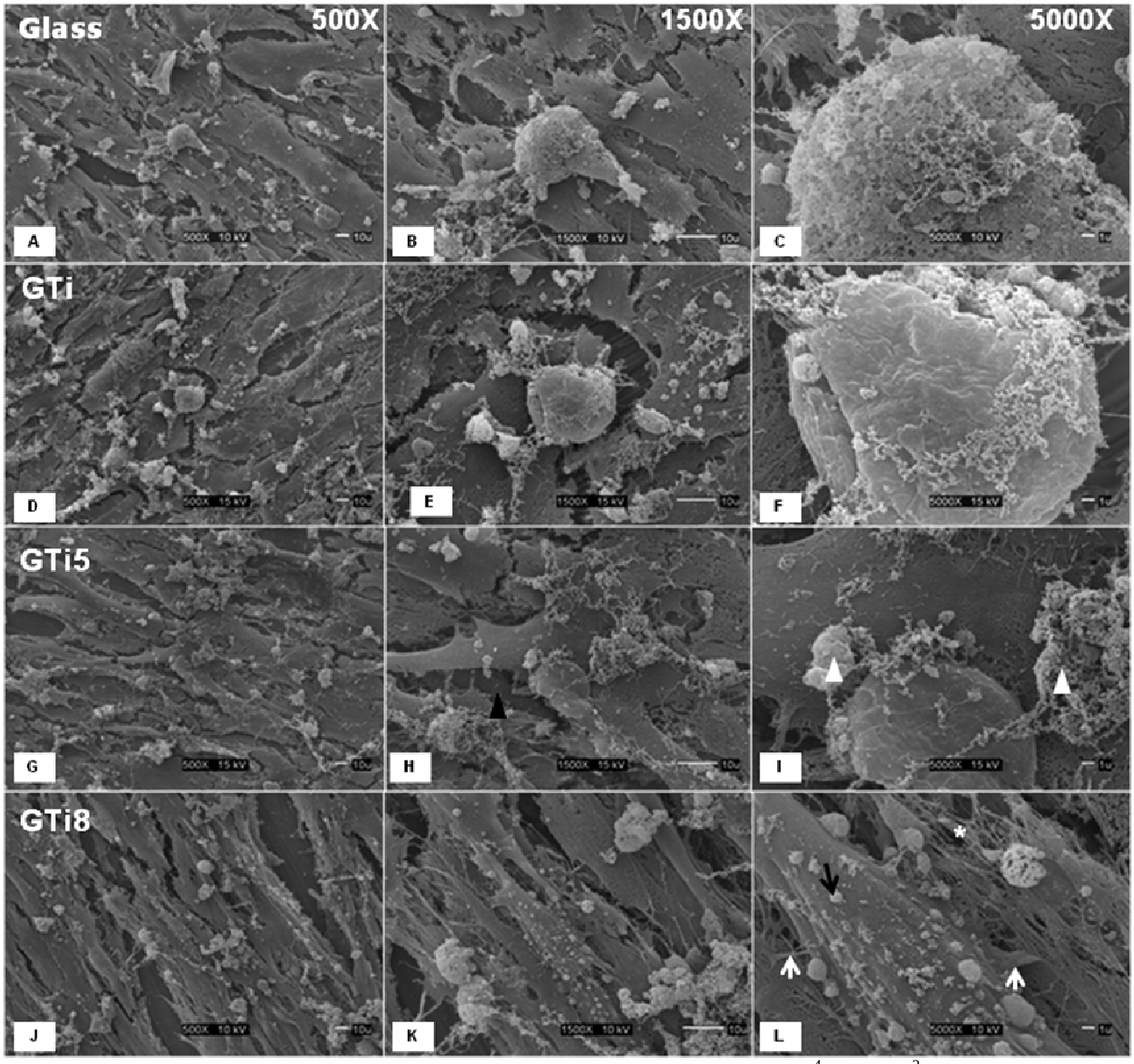

Figure 8. SEM micrographs of hFOB 1.19 cells seeded at a density of 5 x 10^4 cells/cm^2 on a glass coverslip (positive control) (A-C), GTi (D-F), GTi5 (G-I), and GTi8 (J-L) disks and incubated for 14 days (7 days at 33.5ºC and subsequently 7 days at 39.5ºC). Each row shows the cell appearance by SEM on each surface at three magnifications (500, 1500, and 5000X), respectively. Black arrowhead shows the innermost cell of a multilayer; white arrowheads show sponge-like structures that may correspond to nodules of mineralization; black arrow shows a small sphere-like surface evagination on a cell; white arrows show thin cell projections (filopods); the asterisks display fibrous networks that may correspond to collagen fibers. (Scale bar: left and center 10μm, right 1μm).

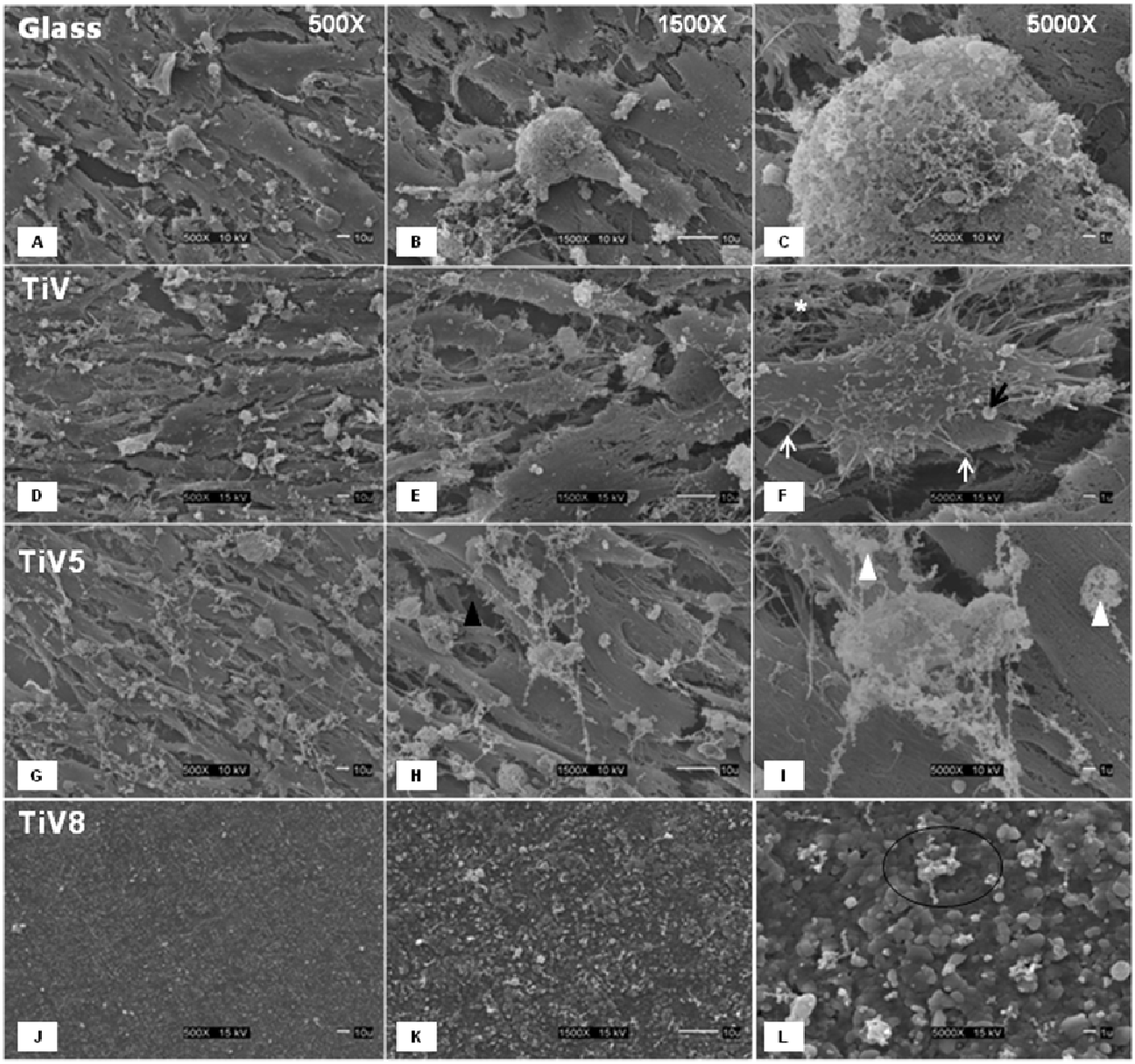

Figure 9. SEM micrographs of hFOB 1.19 cells seeded at a density of 5 x 10^4 cells/cm^2 on a glass coverslip (positive control) (A-C), TiV (D-F), TiV5 (G-I), and TiV8 (J-L) disks and cultured for 14 days (7 days at 33.5ºC and subsequently 7 days at 39.5ºC). Each row shows the cell appearance by SEM on each surface at three magnifications (500, 1500, and 5000X), respectively. Black arrowhead shows the innermost cell of a multilayer; white arrowheads show sponge-like structures that may correspond to nodules of mineralization; black arrow shows a small sphere-like surface evagination on a cell; white arrows show thin cell projections (filopods); the asterisk displays fibrous networks that may correspond to collagen fibers. (Scale bar: left and center 10μm, right 1μm).

5.5 IMMUNOFLUORESCENT LABELING

In order to evaluate osteoblast adhesion qualitatively on autoclaved and thermally oxidized gamma-TiAl and Ti-6Al-4V disks, β1 integrin and vinculin, which are components of focal adhesions, were immunostained in hFOB 1.19 cells seeded on the different surfaces. On the positive control glass, the presence of the three fluorescent labels red, green, and blue were observed, indicating the expression of the β1 integrin and vinculin proteins, and the presence of cell nuclei, respectively, on the cells adhered on glass (Fig. 10A). It was observed in some areas the superimposition of the red and green fluorescent signals, indicating the co-localization of the β1 integrin and vinculin proteins in those areas. The cell nuclei (blue) were observed for the negative control, both isotype controls, and the primary and secondary antibody controls on glass. Some low intensity fluorescence signals at the wavelength of emission of Rhodamine (573 nm) were also observed. However, at the wavelength of emission of Alexa Fluor 647 ® no fluorescent signal was observed (Fig. 10B-F)

Both the metal and the cellular autofluorescence were measured on one set of GTi, GTi5, GTi8, TiV, TiV5, and TiV8 disks, where osteoblast cells were cultured and incubated as described for the experimental samples. However, during the immunofluorescence labeling process of these samples, blocking solution was added instead of primary and secondary antibodies. The presence of cells for the samples used as controls of the metal and cellular autofluorescence was demonstrated with DAPI stain of cell nuclei (Fig. 11). The metal and the cellular autofluorescence values were subtracted from the corresponding experimental fluorescence intensity of samples at the wavelengths of emission of Alexa Fluor 647 ® and Rhodamine, respectively. The data of fluorescence intensity of experimental samples before and after the subtraction of the autofluorescence are presented in Table 1. The images displayed in Figure 12 correspond to images without the autofluorescence.

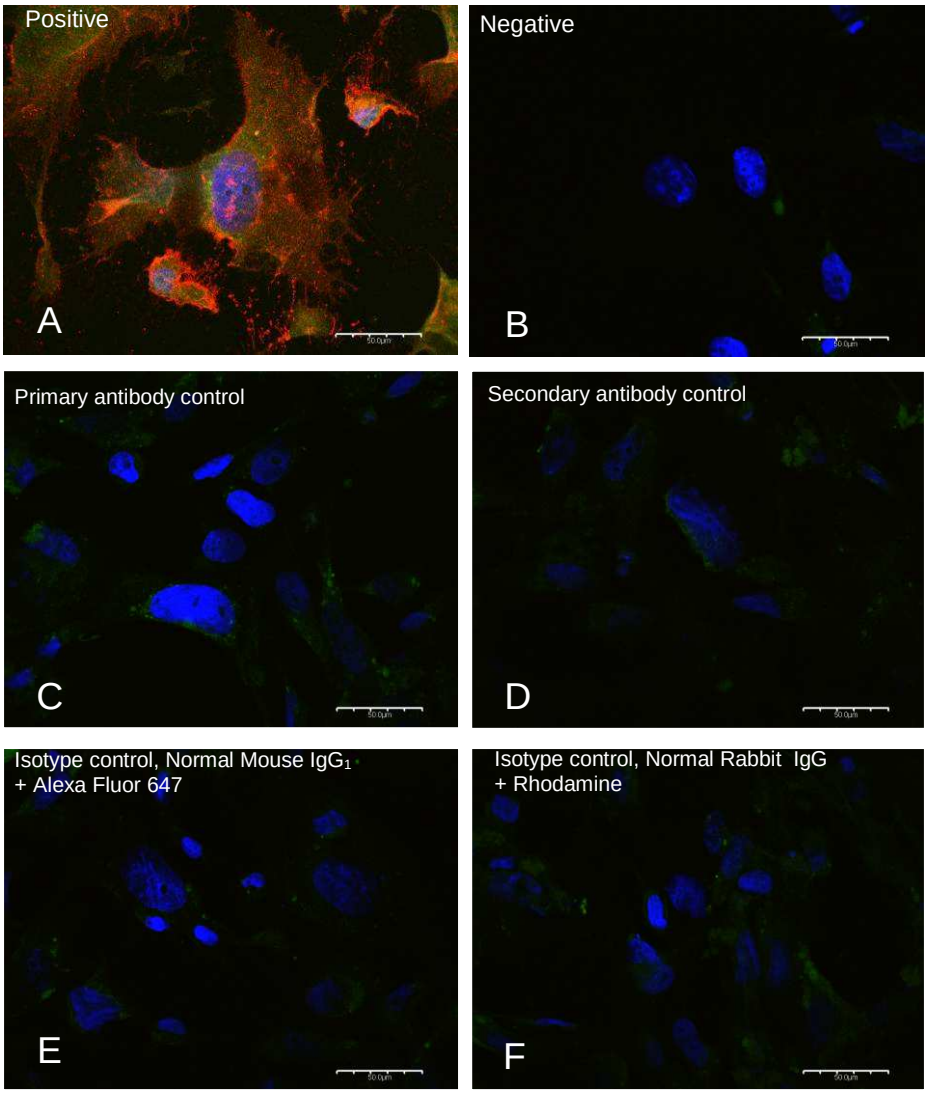

Figure 10. Controls on glass coverslips used for the experiment of immunolabeling of vinculin (Rhodamine labeled, green) and β1 integrin (Alexa Fluor 647® labeled, red) in hFOB 1.19 cells. Cell nuclei were stained with DAPI. hFOB 1.19 cells were seeded on glass coverslips and processed as described in Materials and Methods for positive control (A), negative control (B), primary antibody control (C), secondary antibody control (D), isotype control for primary antibody raised in mouse (E), and isotype control for primary antibody raised in rabbit (F). (60X magnification, scale bar: 50μm).

The immunofluorescent analysis of the expression of adhesion proteins in hFOB 1.19 cells adhered on GTi, GTi5, GTi8, TiV, TiV5, and TiV8 surfaces clearly revealed the presence of the fluorescent labels red, green, and blue, indicating the expression of β1 integrin and vinculin, and the presence of cell nuclei, respectively, in cells adhered on all the surfaces tested, except on TiV8 (Figs. 12 A-R). Osteoblast cells were immunoreactive for β1 integrin, exhibiting cell surface labeling with some scattered brighter cell areas (Figs. 12 B,E,H,K,N,Q). Osteoblast cells were also immunoreactive for vinculin, which exhibited a homogeneous cytoplasmic

(including cell projections) localization displaying a grainy pattern (Figs. 12 A,D,G,J,M,P). However, no defined focal adhesions structures were observed in cells adhered on any surface. In the merged images displayed in Figs. 12 C,F,I,L,O some areas of co-localization of β1 integrin and vinculin were observed, as evidenced by changes in the original color (red or green to orange or yellow). It was also noticed that the β1 integrin was localized at the cell periphery compared to vinculin (white arrow, Fig. 12C), which was localized more centrally (white arrowhead, Fig 12C).

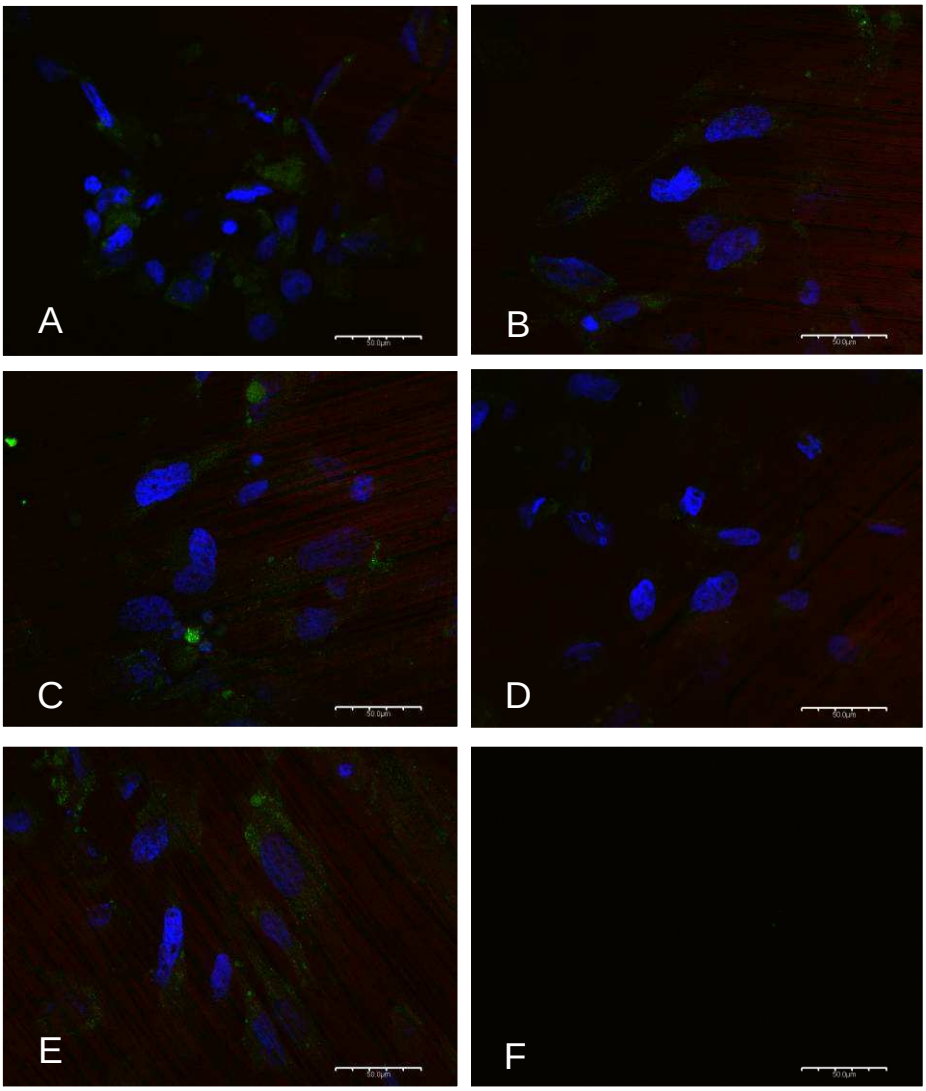

Figure 11. Confocal Laser Scanning Microscopy of metal and cellular autofluorescence controls. hFOB 1.19 cells were seeded on GTi (A), TiV (B), GTi5 (C), TiV5 (D), GTi8 (E), and TiV8 (F) surfaces, incubated for 7 days and processed for immunofluorescent labeling using blocking solution instead of antibodies. Cell nuclei were stained

with DAPI. The metal and the cellular autofluorescence were measured on each sample at 668 nm and 573 nm, respectively. (60X magnification, scale bar: 50μm).

There were no apparent differences in the level of β1 integrin and vinculin expression between cells cultured on GTi, GTi5, GTi8, TiV, and TiV5 disks (Figs. 12A-O), suggesting that hFOB 1.19 cells adhered on GTi, GTi5, GTi8, TiV, and TiV5 disks in a similar manner. In addition, there were no noticeable differences in the cell morphology of the osteoblast cells cultured on the different surfaces tested. In general, the cells exhibited a polygonal (white arrowhead, Fig 12L), elongated (yellow arrow, Fig. 12I), rounded (yellow arrowhead, Fig. 12O), or spindle-shaped (asterisk, Fig. 12F) morphology. No apparent Alexa Fluor 647®, Rhodamine or DAPI fluorescent signals were observed on TiV8 samples (Fig. 12R). However, the measurement of fluorescence intensity of TiV8 surface using the FluoView 4.3 software indicated the presence of very low intensity fluorescence at 668 nm (emission lengthwise of Alexa Fluor 647®) and 573 nm (emission lengthwise of Rhodamine) but no fluorescence at 488 nm (emission lengthwise of DAPI) (Table 1).

Table 1. Fluorescence intensity of β1 Integrin (labeled with Alexa Fluor 647® [668 nm] and vinculin (labeled with Rhodamine [573 nm]) proteins expressed in human osteoblast cells (hFOB 1.19 cell line) cultured for 7 days on GTi, GTi5, GTi8, TiV, TiV5, and TiV8 surfaces, and metal and cellular autofluorescence intensities subtracted from experimental samples.

Substrate	Metal auto-fluorescence (668 nm)	Cellular auto-fluorescence (573 nm)	Initial Fluorescence Intensity (Arbitrary Units*)		Final Fluorescence Intensity (Arbitrary Units)	
			β1 Integrin (668 nm)	Vinculin (573 nm)	β1 Integrin (668 nm)	Vinculin (573 nm)
GTi	**11.554**	**7.218**	**42.33**	**23.673**	**24.180**	**16.660**
GTi5	**16.550**	**8.718**	**40.603**	**22.934**	**24.106**	**14.616**
GTi8	**19.935**	**8.982**	**39.949**	**21.763**	**21.488**	**14.062**
TiV	**18.980**	**7.429**	**44.241**	**24.063**	**20.518**	**16.594**
TiV5	**16.455**	**6.554**	**41.764**	**25.429**	**21.146**	**18.803**
TiV8	**6.418**	**5.166**	**8.72**	**6.16**	**2.081**	**1.027**

* The fluorescence intensity was measured using the Fluoview Version 4.3 Software (Olympus Corporation) in arbitrary units (a.u.) that ranged from 0 to 255. The 0 represented the lack of signal (black area) and the 255 represented the brightest fluorescent signal.

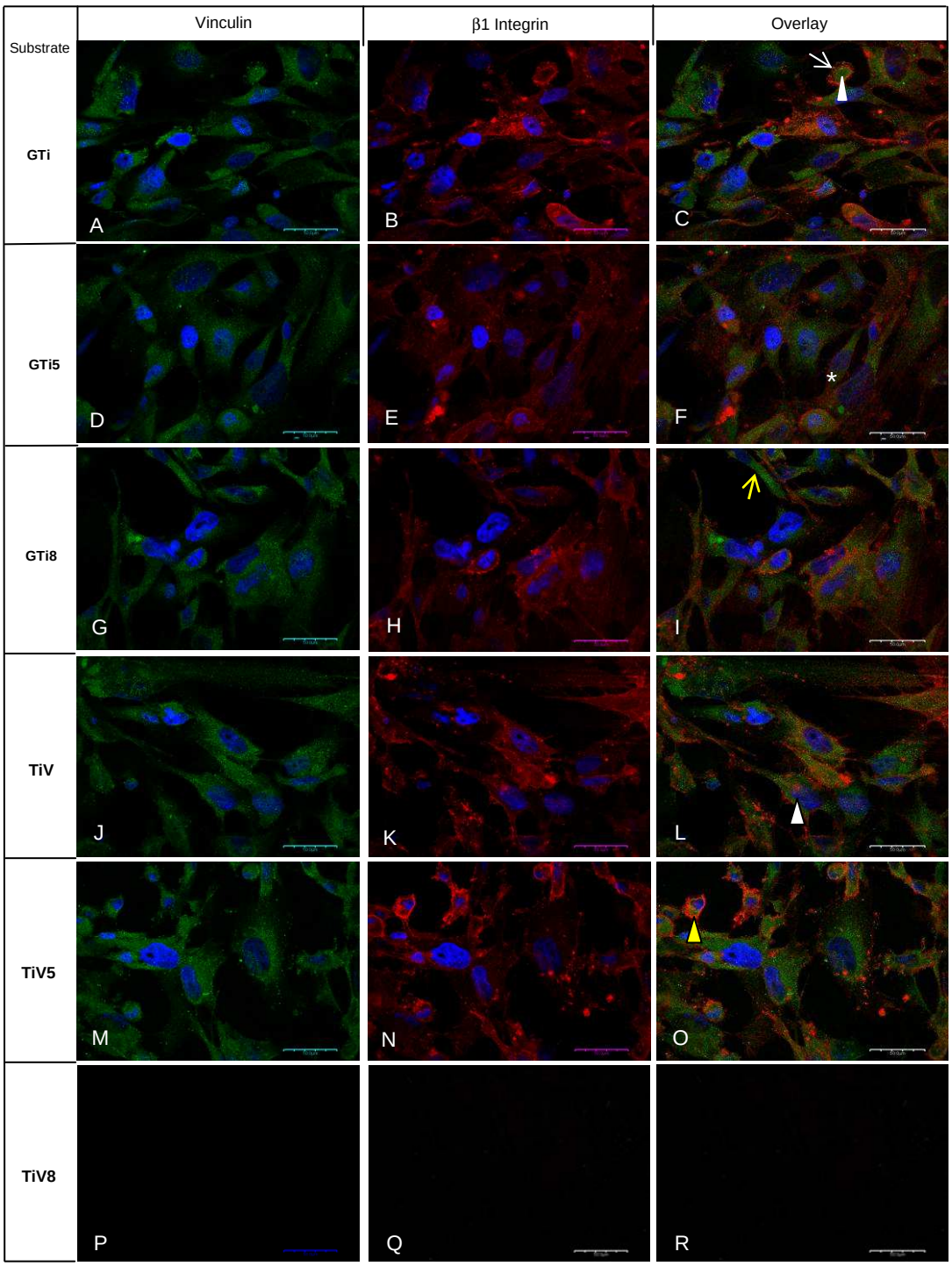

Figure 12. Confocal Laser Scanning Microscopy of the expression of vinculin (Rhodamine labeled, green) and β1 integrin (Alexa Fluor 647® labeled, red) in hFOB 1.19 cells cultured for 7 days on autoclaved (GTi,TiV) and thermally oxidized at 500ºC (GTi5, TiV5) and 800ºC (GTi8, TiV8) gamma-TiAl and Ti-6Al-4V surfaces. Cell nuclei were stained with DAPI. Each row shows the expression of vinculin (first column), β1 integrin (second column) and the corresponding merged image (third column) in each surface tested: GTi (A-C), GTi5 (D-F), GTi8 (G-I), TiV (J-L), TiV5 (M-O), TiV8 (P-R). White arrow shows cell periphery, white arrowhead shows the central portion of a cell, the asterisk shows a spindle-shaped cell, the yellow arrow shows an elongated cell, white arrowhead shows a polygonal cell and yellw arrowhead shows a rounded cell. (60X magnification, scale bar: 50μm).

6 DISCUSSION OF RESULTS

The *in vivo* (6) and the *in vitro* (7) biocompatibility of the potential biomaterial gamma-TiAl (Ti-48Al-2Cr-2Nb [at.%]) was demonstrated previously (6,7). However, the response of osteoblast cells to thermally oxidized gamma-TiAl surfaces has not been addressed to date. The main goal of this research was to evaluate the human osteoblast cell adhesion on thermally oxidized gamma TiAl surfaces in order to determine its biocompatibility, and in the long term its possible usefulness as a biomaterial for orthopedic applications. The biocompatibility of a material is defined as the capacity of the material to perform with an appropriate host response in a specific application (27). As cell adhesion is the first event of cell/material interactions, *in vitro* evaluation of the capacity of attachment of bone forming cells on materials for orthopedic applications is necessary to determine its biocompatibility. The posterior competence of cells to proliferate and differentiate on contact with the substrate will depend on the initial cell adhesion (23).

In this research, the ability of the human fetal osteoblast-like cells (hFOB 1.19 cell line) to adhere and proliferate on autoclaved (GTi, TiV) and thermally oxidized at 500°C (GTi5, TiV5) and 800°C (GTi8, TiV8) gamma-TiAl and Ti-6Al-4V disks respectively, was evaluated both quantitatively and qualitatively. The hexosaminidase assay was used to quantitatively assess the cell adhesion on the different surfaces tested whereas Scanning Electron Microscopy (SEM) and immunofluorescence labeling of β1 integrin and vinculin were used to qualitatively assess the cell adhesion. The hexosaminidase assay is based on the activity of the enzyme N-acetyl-β-D-hexosaminidase also known as β-N-Acetylglucosaminidase (EC 3.2.1.52), which is a ubiquitous lysosomal enzyme in mammalian cells that takes part in intracellular degradation of glycolipids and glycoproteins (55). Landegren (55) proposed the hexosaminidase assay to estimate the cell numbers in different biological assays. One application tested by Landegren was the indirect measurement of rat primary hepatocyte attachment to microtiter wells that had been coated with fibronectin (55).

The hexosaminidase assay has been used by different scientists to quantify cell attachment and proliferation on diverse substrates. Neitmann *et al.* (61) evaluated melanocyte cell attachment on 96 well plates coated with fibronectin, laminin or collagen after ultraviolet

(UV) irradiation, using the hexosaminidase assay (61). Givens *et al.* (62) compared the sensitivity of hexosaminidase, MTT (3-[4,5-dimethylthiazol]-2-yl-2,5-diphenyl tetrazolium) and neutral red assays to screen potential antiproliferative drugs on cultured fibroblasts. Although the three colorimetric methods showed strong linear relationship between optical density and Coulter-cell counts, the hexosaminidase assay was far more sensitive, reliably detecting only a few hundred cells (62). May *et al.* (69) compared the number of keratinocyte cells adhered on different substrates by either the hexosaminidase or a fluorogenic assay. The fluorescent probe used was 5,6-carboxyfluorescein diacetate succidimyl ester (CFDA-SE). They found that the overall trends in adhesion were similar by both assessment methods. However, it was demonstrated that pre-labeling of keratinocytes with CFDA-SE may affect cellular functions such as adhesion and even proliferation (69).

Advincula *et al.* (56) evaluated the adhesion of MC3T3-E1 osteoblast-like cells on passivated and sol-gel coated Ti-6Al-4V surfaces using the hexosaminidase assay. McDonald *et al.* (8) evaluated the attachment of MG63 osteoblast-like cells on Ti-6Al-4V disks submitted to different thermal and chemical surface treatments, using the hexosaminidase assay. They used a standard curve of hexosaminidase activity versus cell number (from 10000 to 150000 measured by a Coulter counter) to extrapolate the cell number in the experimental ("unknown") wells based on the hexosaminidase activity. They found a strong relation between the hexosaminidase activity and cell number demonstrated by a mean correlation coefficient (r^2) of 0.95 and above.

In the present study, standard curves were used to extrapolate the cell number on experimental disks based on the hexosaminidase activity. Three standard curves were prepared, one for each of the three independent hexosaminidase experiments performed in this study (Appendix A). Human fetal osteoblasts of the cell line hFOB 1.19, ranging from 500 to 55000 viable cells per well, were seeded in 96-well plates and incubated for 24h at 39.5°C. The cell viability was determined by the trypan dye exclusion test. Although there was a linear relationship between the hexosaminidase activity and cell number in the three standard curves (r^2 = 0.876, 0.8085, and 0.9238 for standard curves of experiment 1, 2, and 3, respectively), the data fitted a cubic model more accurately. The r^2 of the standard curves fitted to the cubic model were 0.9945, 0.9964, and 0.9989, respectively (Appendix A). When the estimated cell numbers obtained with the linear model were compared with those obtained with the cubic model, it was observed that the linear model was overestimating the data.

In the present study, human osteoblast adhesion on GTi, TiV, GTi5, TiV5, GTi8, and TiV8 surfaces was evaluated at 24h (1 day), 7 and 14 days post-seeding using the hexosaminidase assay. There were no significant differences in the number of osteoblast cells attached on the different surfaces tested after 1 day of incubation. However, the number of cells attached on TiV8 was significantly lower than the number of cells attached on the other surfaces tested (GTi, TiV, GTi5, TiV5, and GTi8) after 7 and 14 days of incubation. In addition, it was observed that the number of cells attached on TiV8 decreased over time. This particular behavior of hFOB 1.19 cells on TiV8 was the cause of the significant interactions found between the factors tested (type of metal, time of incubation, and temperature of oxidation) when the data of the hexosaminidase assay were analyzed by means of a factorial ANOVA (Appendix C1). This fact was corroborated when a new factorial ANOVA was performed omitting the data of the cell number attached on TiV8 and GTi8 surfaces, which did not yield significant interactions between the factors tested (Appendix C2).

The hexosaminidase assay also showed that the number of cells adhered on all the surfaces tested increased from day 1 to 7, and after this time the number of cells remained relatively constant, except on TiV8. These results suggest that the cells initially attached at day 1 on all the surfaces were able to proliferate until day 7, except on TiV8. After this time they remained in a relatively constant number until day 14. This was the expected result, since the hFOB 1.19 cells were incubated until day 7 at a permissive temperature (33.5ºC). Then the samples were changed to a restrictive temperature (39.5ºC) for 7 additional days. At permissive temperatures or as subconfluent cultures, hFOB 1.19 cells exhibit rapid cell division whereas at restrictive temperatures or at confluence, the hFOB 1.19 cell division is slowed down and differentiation increases. This particular behavior of the human fetal osteoblast cell line 1.19 (hFOB 1.19) is due to the presence in its genome of a transfected gene coding for a temperature-sensitive mutant (tsA58) of the SV40 T antigen (17-19). Expression of T antigen in human cells results in an increased rate of proliferation when it interacts with the retinoblastoma gene product Rb. Under conditional immortalization, the mutant T antigen is only active (immortalizes cells) at the permissive temperature. Thus, the return to a nonimmortalized state can be manipulated by changing the incubation of the cells to a restrictive temperature (17-19).

The hFOB 1.19 cells (human fetal osteoblast cell line 1.19) were used in this research because of their ability to differentiate into mature osteoblasts and the possibility of being

subcultured for a long period of time due to their immortality. This cell line is immortalized but non-transformed, displaying minimal chromosome abnormalities and a normal spectrum of matrix proteins. Although primary-human osteoblasts have a normal osteoblastic phenotype, these cells typically have complex nutritional requirements *in vitro*, grow very slowly, and have a limited life span when successfully brought into culture. Transformed human osteosarcoma cell lines are not the best choice to study osteoblast cells-substrates interactions owing to the fact that they do not exhibit the complete phenotype of differentiated osteoblasts, have abnormal growth properties, and exhibit response to hormones and cytokines that sometimes differ from those of primary cultures (17-19,26).

Some of the cell adhesion studies on thermally oxidized metallic surfaces (8,11,12,53,54) and on other substrates (34,56,63,64) have been short-term adhesion studies (15 min until 24 or 48h) instead of studying cell attachment over longer periods of time, which could be more representative of the *in vivo* conditions. In this study, the evaluation of early cell attachment (at 24h) on TiV8 provided only limited information about its biocompatibility. At this time point, the hexosaminidase assay did not detect significant differences in cell attachment among TiV8 and the other surfaces tested. However, the number of cells attached on TiV8 was significantly lower compared to the other surfaces tested (GTi, TiV, GTi5, TiV5, and GTi8) after 7 and 14 days of incubation. This finding suggests that cells were initially able to attach on TiV8, but TiV8 did not exhibit osteoconductive properties. On the contrary, the behavior of hFOB 1.19 cells in contact with the TiV8 surface suggests that the oxide layer formed on Ti-6Al-4V by thermal oxidation at 800ºC exhibits cytotoxic effects either allowing the release of harmful ions like vanadium (V) or aluminum (Al) from the bulk alloy in a time dependent manner, or by direct effect of toxic compounds formed in the oxide layer during the thermal oxidation. The surface oxide formed on TiV8 appears to be a thick (~10μm) and porous titanium oxide (rutile) layer (4). Delgado-Alvarado and Sundaram (4) determined that this oxide layer provided less corrosion resistance to Ti-6Al-4V *in vitro* than the oxide layer formed by autoclaving for 1h (4). Garcia-Alonso *et al.* (12) found that thermal oxidation at 700ºC for 1h originates an oxide layer of rutile with small Al_2O_3 nuclei. They determined by electrochemical impedance spectroscopy that these alumina nuclei with a lower corrosion resistance could act as easy diffusion paths toward the surface (12). Thus the slow and continuous release of harmful ions from the bulk alloy (Ti-6Al-4V) to the surface through the pores of the titanium oxide or the alumina nuclei,

remains as a possible explanation for the lack or the small number of cells adhered on TiV8 at 7 and 14 days postseeding.

Most thermal oxidation studies of Ti-6Al-4V have not reported significant amounts of V in the oxide layers compared to the non oxidized surfaces (9,11,12,14,66). However, McDonald *et al.* (8) found that the Al and the V levels in thermally oxidized Ti-6Al-4V samples were significantly higher than those determined for the control disks (non-oxidized). They reported the presence of V as both VO_2 and V_2O_5 on thermally oxidized (600ºC for 1h in either air or pure oxygen) Ti-6Al-4V samples. The V_2O_5 was twice as prevalent as VO_2 within the surface oxide layer. However, the levels of V found in the oxide layer did not affect the MG63 cell attachment on Ti-6Al-4V samples (8). Thermal oxidation (550ºC for 1h) of the experimental alloy Ti-1.5Al-25V generates an oxide layer of approximately 100 nm composed of rutile and crystalline vanadium pentaoxide (V_2O_5) (13). Vero-fibroblasts seeded for 7 days on this surface displayed different morphological alterations, and showed a decreased proliferation and viability. Additionally, the cells decreased their spreading area compared to cells grown on Ti samples (13).

The chemical composition of the surface oxides formed on autoclaved and thermally oxidized gamma-TiAl and Ti-6Al-4V surfaces obtained in the experimental conditions of this research are being studied by X-Ray Photoelectron Spectroscopy (XPS) by Dr. Esteban Fachini, a collaborator of our research group, to determine if any compound associated with cytotoxicity is formed specifically on TiV8. In addition, cytotoxicity tests will be performed for the thermally oxidized gamma-TiAl and Ti-6Al-4V surfaces to determine if any ion or compound is being released abnormally to the culture medium that could be responsible of the cytotoxic effects observed on TiV8.

There is not much agreement about the effects of thermal oxidation of Ti or its alloys on osteoblast cell adhesion. The present research is in agreement with some studies that have reported lack of significant differences among cell attachment on control metallic surfaces (polished but non thermally oxidized) compared with the thermally oxidized surfaces (12,54). On the other hand, Feng *et al.* (53) found that cell adhesion was greater on heat treated cp-Ti samples compared to control surfaces (non heat-treated) after 24h of incubation. McDonald *et al.* (8) observed that cell attachment was increased on thermally oxidized (600ºC for 1h in either air

or pure oxygen) Ti-6Al-4V surfaces pretreated with fibronectin 0.1 nM, after 2h of incubation. However, they did not find significant differences in cell attachment among the thermally oxidized and non oxidized Ti-6Al-4V uncoated samples (8). Other researchers, in time-course cell adhesion experiments, have reported increased numbers of osteoblast cells attached on the cpTi or Ti-6Al-4V thermally oxidized surfaces in all (52) or in some of the specific time points tested (9,11).

It has been suggested that the highly polar (anionic) oxides formed by thermal oxidation on Ti alloys originates a more hydrophilic surface that attract a variety of cations (like calcium ions), which then bind electrostatically to proteins involved in cell adhesion (like fibronectin), thus enhancing cell attachment (8,52). Sousa *et al.* (60) evaluated fibronectin adsorption on cpTi surfaces covered by titanium oxide (TiO_2). TiO_2 is an oxide found frequently on thermally oxidized cp-Ti and Ti-6Al-4V surfaces. They observed that fibronectin partially covered the surfaces tested after 10 min. The fibronectin formed globular aggregates or ellipsoids that coalesced, forming clusters as the time of adsorption and the concentration increased, reaching a maximum after 60 min of incubation. They suggested that the fibronectin aggregates formed on the TiO_2 surfaces promoted cell adhesion and cytoskeleton organization (60). In the present study, some irregular structures were observed by SEM on both metals (gamma TiAl and Ti-6Al-4V) autoclaved and incubated for 14 days with culture medium but without cells (control surfaces). These structures were not observed on the surfaces autoclaved without incubation with culture medium suggesting that this corresponds to precipitation of the culture medium components.

McDonald *et al.* (8) suggested that the increased Al_2O_3 content on the thermally oxidized Ti-6Al-4V surface pretreated with 0.1 nM fibronectin was responsible for the enhanced cell attachment. They suggested that the Al enriched surface layer may influence protein conformation potentially exposing cellular binding domains, thus facilitating cell attachment. Saldaña *et al.* (11) also related the increased surface Al content with the enhanced adhesion of osteoblasts on thermally oxidized (500ºC, 1h) alumina blasted Ti-6Al-4V surfaces compared to the number of cells attached on the blasted and non-oxidized Ti-6Al-4V surfaces. Previously, it was suggested that thermal oxidation for 1h in air at 500ºC of the gamma-TiAl alloy of composition Ti-48Al-2Cr-2Nb (at.%) originates a continuous blue colored oxide layer of Al_2O_3 whereas at 800ºC originates a dark yellow multilayered scale constituted by an outer layer of

TiO_2 (rutile), and a combination of TiO_2 and Al_2O_3 in the middle layer (4). Thus an increased cell attachment was expected on the gamma-TiAl surface oxidized at 500ºC due to the presence of the Al_2O_3 oxide layer. However, the methods used to evaluate cell adhesion did not show significant differences in cell attachment between autoclaved, and thermally oxidized at 500ºC or 800ºC gamma-TiAl disks in the experimental conditions employed in this research.

In this study, the changes in morphology of hFOB 1.19 cells on glass coverslips throughout different time periods of culture (1, 3, 5, 7, 14, 21 and 28 days) were studied using SEM to establish a baseline for comparison purposes. It was found that the hFOB 1.19 cells from day 1 to day 28 exhibit mainly elongated and polygonal shapes. However, at all time points some cells showed variable appearance (spherical, oval, or spindle-shaped). At early times of culture (from day 1 until day 5) the cells were flattened exhibiting numerous filopodia and lamellipodia, indicating that they were actively spreading. After 7 days of culture confluent multilayers were observed. The presence of a few nodules of mineralization (small rounded structures with sponge-like morphology) presumably represented the onset of the mineralization process. From day 14 to day 28 the maturation of the extracellular matrix (ECM) is evidenced by the presence of fibrous networks associated with cells and the increase in nodules of mineralization. The fibrils observed may correspond to fibrillar collagen, the main component of the bone ECM.

The results of this study agree with the programmed developmental sequence that leads to the differentiation of hFOB 1.19 cells in culture, described by Harris *et al.* (17). This sequence is characterized by an early proliferative stage, during which osteoblastic cells are relatively undifferentiated, and later postconfluent stages, which involve the expression of bone cell phenotypic markers and ultimately extracellular matrix mineralization (17). The morphology of hFOB 1.19 cells on glass coverslips observed in this study up to day 3 agree with the hFOB 1.19 cell morphology on hydrophilic surfaces described for Liu *et al.* (26). They described the hFOB 1.19 cells after 24h of incubation on hydrophilic surfaces as elongated and flattened, fully spread and in contact by extending filopodia. After 48h, cell rounding associated with cell division was observed. Additionally, on hydrophobic surfaces the cells retained a spindle-shaped morphology up to 96h.

In this study, cell adhesion on the different surfaces (GTi, TiV, GTi5, TiV5, GTi8, and TiV8) was qualitatively evaluated by SEM. SEM images showed that after 14 days of incubation (7 days at 33.5ºC and subsequently 7 days at 39.5ºC) hFOB 1.19 cells were attached to the surface of GTi, GTi5, GTi8, TiV and TiV5 disks, but they were not adhered on TiV8 disks. No apparent morphological differences of hFOB 1.19 cells grown on GTi, GTi5, GTi8, TiV and TiV5 surfaces were observed. Cells were mainly elongated and polygonal, although some cells showed variable appearance (spherical, oval or spindle-shaped) with many filopodia. Some cells exhibited dorsal vesicles and ruffles demonstrating extensive cellular activity. At this time confluent multilayers on all samples covering the residual grooves resulting from the polishing process were observed. The presence of nodules of mineralization (small rounded structures with sponge-like morphology) and fibrous networks suggesting the maturation of the ECM and the formation of a bone-like tissue was also observed on all the surfaces, except on TiV8. On TiV8 samples, only small irregular structures that may correspond to cellular debris were observed 14 days post-seeding, suggesting that hFOB 1.19 cells were able initially to attach to the thermally oxidized at 800°C Ti-6Al-4V surface, but cells did die in a time dependent manner, and after 14 days of incubation only remaining cellular structures were present on this surface. Taken together, these findings suggest that hFOB 1.19 cells were able to adhere and differentiate into mature osteoblast cells on all surfaces studied, except on TiV8. Cell appearance of hFOB 1.19 cells cultured for 14 days on the different gamma-TiAl and Ti-6Al-4V surfaces, except on TiV8, was similar to that observed on time matched glass coverslips, suggesting that surface oxides produced by thermal oxidation at 500°C and 800°C on gamma-TiAl and at 500°C on Ti-Al-4V did not modify hFOB 1.19 cell morphology. However, it may be necessary to seed a lower number of hFOB 1.19 cells on the surfaces than those used in this study (5×10^4 cells/cm^2) to determine slight variations in cell morphology on contact with substrates such as the number of cell projections, presence of surface vesicles, etc.

Studies of osteoblast response to thermally oxidized Ti-6Al-4V surfaces have not included SEM assays to determine the cell morphology variability in response to the different surface oxides (8,9,11,12). However, other studies have determined the differences in osteoblast cell morphology and adhesion according to surface topography (45, 65). Anselme *et al.* (45) observed that human primary osteoblasts had a stellate shape with numerous filamentous extensions on less organized surfaces such as that processed by sandblasting. The osteoblasts

were not able to attain confluence, even after 14 days of incubation because they displayed a lower proliferation rate on the sandblasted surface. On the contrary, the cells were flattened and oriented in a parallel way on glass, attaining confluence after 14 days. Sader *et al.* (65) evaluated murine primary osteoblast adhesion on Ti surfaces with different roughnesses. They observed that adhesion and spreading rates were different and depended on surface microtopography. On the roughest surface osteoblasts did not spread completely and remained polygonal whereas on the smoothest surface cells were widely spread over with flattened morphology and orientation following surface grooves, after 48h of incubation.

Zhao *et al.* (70) found significant differences in the number of cells attached on Ti surfaces with different surface energy and roughness. They found that the number of MG63 osteoblasts attached on the sandblasted and acid etched samples (complicated three-dimensional topography) decreased by 44% compared to smooth Ti surface (70). In this study, the surface roughnesses of the different samples were not measured. However, the SEM images of GTi8 and TiV8 without cells exhibited a rougher surface compared to the other samples. Bigger oxide granules were present on TiV8 compared to those of GTi8 that conferred an irregular appearance to this surface. In addition, this oxide layer covered the parallel grooves and striations that are still visible on GTi8, suggesting that TiV8 oxide layer is thicker than the other oxide layers evaluated. One plausible explanation for the lower cell attachment observed on TiV8 could be its rough and irregular surface, which did not promote a tight cell adhesion at day 1, thus favoring cell detachment in a time dependent manner and the consequent lack of cells on TiV8 at 7 and 14 days postseeding.

The hFOB 1.19 cell adhesion on the different surfaces was also qualitatively evaluated using specific antibodies against the adhesion proteins β1 integrin and vinculin after 7 days of incubation. Osteoblast cells were immunoreactive for β1 integrin exhibiting cell surface labeling with some scattered brighter cell areas located at the cell periphery. hFOB vinculin immunoreactivity was observed as homogeneous cytoplasmic localization displaying a highly punctate or grainy pattern, but not as bright, short, and dense patches as have been described in immunofluorescence analyses (44,57). That is, no well defined focal contacts were observed on any surface tested.

The labeling results for the negative controls used in this experiment demonstrated the specificity of both primary and secondary antibodies. However, the labeling pattern of β1 integrin and vinculin in this experiment suggests that primary antibodies are not specific for β1 integrin and vinculin present in focal contacts. It appears that the monoclonal antibody anti integrin β1 MAB1987Z (Chemicon), which was directed against an extracellular epitope, reacts not only with the β1 integrin subunits located in focal contacts but it reacts with the β1 integrin subunits in the whole cell membrane. The brighter cell areas labeled with anti integrin β1 may correspond to focal contact sites, where the integrins are clustered after cell adhesion. The homogeneous cytoplasmic immunoreactivity of vinculin may be explained by the lack of specificity of the rabbit anti-human vinculin polyclonal antibody SC-5573 (Santa Cruz Biotechnology) that may be reacting with the vinculin located in focal contacts as well as with the vinculin cytoplasmic soluble fraction. In addition, the permeabilization of the cells with saponin may be responsible in part of the homogeneous pattern of labeling using the anti-vinculin antibody. When Meyer *et al.* (57) used saponin to permeate the osteoblasts for indirect immunofluorescent labeling of vinculin, they exhibited a diffuse cytoplasmic pattern whereas cells permeated with the non-ionic detergent Triton X-100 before methanol fixation and subsequent immunostaining abolished nearly the entire homogeneous fluorescent pattern (57). They suggest that Triton X-100 is effective to remove the vinculin cytoplasmic fraction, which was thought to be predominantly soluble vinculin.

The lack of DAPI and β1 integrin signals on TiV8 suggest that no cells were present on this surface after 7 days of incubation. It would be interesting to determine in new experiments, if some cells are present on this surface after 1 day of incubation to compare the results of the immunofluorescent labeling experiments with those of the hexosaminidase assay. Taken together, the results of the immunofluorescent experiments indicated that hFOB 1.19 cells expressing the cell adhesion proteins, β1 integrin and vinculin, were present on the different surfaces tested, except on TiV8, 7 days postseeding. The focal contact sites appear to be located at the cell periphery, where β1 integrin and vinculin were co-localized (yellow areas).

Focal adhesion structure development at cell-biomaterial interfaces is closely related to cell adhesion and further cell function (68). At focal adhesions, bundles of actin filaments (stress fibers) are anchored to receptors of the integrin family through a multi-molecular complex of

junctional plaque proteins. For this reason, most studies that evaluate cell/substrate interactions, including cell adhesion, use integrins and/or vinculin proteins as adhesion markers (9,44-46). Frequently, they also label the actin filaments to study the organization of the cytoskeleton according to the surface tested and its relation with the focal adhesion contacts. When cell adhesion is evaluated on different substrata, both the immunoreactivity and the formation of stress fibers and vinculin plaques are studied to determine the maturation of the focal adhesion structures (44,68). For this reason, it is recommended that the co-localization of adhesion cell markers such as vinculin, talin, paxillin, etc and actin filaments to establish differences in the adhesion capability of hFOB 1.19 cells on the different surfaces evaluated in this experiment are determined.

Neither the quantitative data from the hexosaminidase assay nor the qualitative data from the SEM and the immunofluorescent detection of adhesion proteins (β1 integrin and vinculin) showed apparent differences in the amount of cells adhered on any of the gamma-TiAl surfaces evaluated (autoclaved and thermally oxidized at 500°C or 800°C) as well as on the autoclaved and thermally oxidized at 500°C Ti-6Al-4V surfaces. These results suggest that gamma-TiAl surfaces are biocompatible and have the potential for being used as implant materials. Furthermore, the results of the hexosaminidase assay, the SEM and the immunofluorescent analyses of cell adhesion proteins indicate that the Ti-6Al-4V surface which is thermally oxidized at 800°C displays cytotoxic effects on hFOB 1.19 cells in a time dependent manner. These results are not in agreement with Saldaña *et al.* (9) who determined that cell attachment increased on thermally oxidized (at 500°C and 700°C 1h in air) Ti-6Al-4V surfaces compared to polished Ti-6Al-4V surfaces. However, they found that the viability and the proliferation on the surface thermally oxidized at 700°C were significantly less compared with the polished and the thermally oxidized at 500°C surfaces, after 3 days of incubation. However, after 7 days of incubation these differences had disappeared (9). The results of this study are opposed to those of García-Alonso *et al.* (12) who determined that the percentage of attachment after 1 and 2h of culture was significantly greater on thermally oxidized at 700°C Ti-6Al-4V surfaces than those of Ti-6Al-4V surfaces oxidized at 500°C (12).

The main aim of this study was to investigate the biocompatibility of gamma-TiAl thermally oxidized surfaces. However, a number of points regarding the quantitative analysis of

the expression of proteins used as cell adhesion markers (focal adhesion proteins like vinculin and integrins) for hFOB 1.19 cells seeded on thermally oxidized gamma-TiAl and Ti-6Al-4V disks using Confocal Laser Scanning Microscope need to be further elaborated. Future work must address the issue if the β1 integrin and vinculin labeling patterns observed in this study are indeed due to weak cell adhesion on the substrates or if they are due to primary antibodies non-specific binding to focal adhesion points.

7 CONCLUSIONS

- The hexosaminidase assay showed that there were no significant differences in the number of hFOB 1.19 cells attached on the different surfaces tested after 1 day of incubation. However, the number of cells attached on Ti-6Al-4V thermally oxidized at 800°C was significantly less compared to the number of cells attached on the other surfaces evaluated, 7 and 14 days postseeding.
- Scanning electron microscopy (SEM) demonstrated the presence of hFOB 1.19 cells on all the gamma-TiAl surfaces evaluated (autoclaved and thermally oxidized at 500°C and 800°C surfaces) as well as on autoclaved and thermally oxidized at 500°C Ti-6Al-4V surfaces after 14 days of incubation. However, on Ti-6Al-4V surfaces thermally oxidized at 800°C only irregular structures that resembled cell debris were observed.
- Immunofluorescent labeling assays demonstrated the presence of β1 integrin and vinculin in hFOB 1.19 cells cultured on all the gamma-TiAl surfaces evaluated (autoclaved and thermally oxidized at 500°C and 800°C surfaces) as well as on autoclaved and thermally oxidized at 500°C Ti-6Al-4V surfaces but not on Ti-6Al-4V oxidized at 800°C after 7 days of incubation.
- Immunofluorescent and SEM analyses did not show apparent differences in the morphology of hFOB cells cultured on the different surfaces tested after 7 and 14 days, respectively.
- Taken together, cell adhesion studies indicated that hFOB 1.19 cells were able to attach similarly on the different surfaces tested, except on Ti-6Al-4V oxidized at 800°C (TiV8), at the different times evaluated (1, 7, and 14 days). These results suggest that all tested surfaces but TiV8 are biocompatible.
- Thermally oxidized gamma-TiAl surfaces (at 500°C and 800°C) allowed hFOB 1.19 cell adhesion and displayed no apparent cytotoxic effects on hFOB 1.19 cells, suggesting that these surfaces have the potential to be used as implant materials.

8 RECOMMENDATIONS

To further validate gamma-TiAl as a biomaterial the following studies are recommended:

- Study the chemical composition of the surface oxide layers formed on thermally oxidized gamma-TiAl and Ti-Al-4V surfaces by means of X-Ray Photoelectron Spectroscopy (XPS) to determine the possible relationship between chemical composition and cytotoxicity on thermally oxidized Ti-Al-4V surfaces.
- Perform a cytotoxicity test on thermally oxidized gamma-TiAl and Ti-6Al-4V surfaces by an extraction method to determine if any harmful ion or compound is being released to the culture medium.
- Evaluate the wear resistance *in vitro* of the gamma-TiAl surface oxidized at 500°C, which is possibly a good candidate to be used as an implant material.
- Study the expression of osteoblastic phenotype markers on thermally oxidized gamma-TiAl and Ti-6Al-4V surfaces to determine the cell differentiation capability on these surfaces.
- Use lower cell densities than those used in this study (5×10^4 cells/cm^2) to study slight morphological differences of hFOB 1.19 cells on thermally oxidized gamma-TiAl and Ti-6Al-4V surfaces by SEM.
- Perform a new immunofluorescent assay to determine the co-localization of cell adhesion markers (vinculin, paxillin or talin) with actin-F on the thermally oxidized surfaces to determine the formation and maturation of focal adhesions points on the different surfaces.
- Use monoclonal antibodies specific for vinculin present only in focal adhesions to avoid diffuse immunostaining of cytoplasmatic vinculin in osteoblasts.
- Evaluate the adhesion of hFOB 1.19 cells on thermally oxidized at 800°C Ti-6Al-4V surfaces after 1 and 7 days of incubation by SEM, to corroborate the results of the hexosaminidase assay.
- *In vivo* studies should be performed in order to establish the use of thermally oxidized gamma-TiAl alloys as implants.

9 LITERATURE CITED

1. Woodman, J. L., J. J. Jacobs, J. O. Galante, R. M. Urban. 1983. Metal ion release from titanium-based prosthetic segmental replacements of long bones in baboons: a long-term study. J Orthop Res. 1: 421-430.

2. Khan, M.A., R.L. Williams, D.F. Williams. 1999. The corrosion behaviour of Ti–6Al–4V, Ti–6Al–7Nb and Ti–13Nb–13Zr in protein solutions. Biomaterials 20: 631–637.

3. Singh, R. and N.B. Dahotre. 2007. Corrosion degradation and prevention by surface modification of biometallic materials. J Mater Sci: Mater Med. 18:725–751.

4. Delgado-Alvarado, C., P.A. Sundaram. 2006. Corrosion evaluation of Ti-48Al-2Cr-2Nb (at.%) in Ringer's solution. Acta Biomaterialia 2(6): 701-708.

5. Escudero, M.L., M.A. Muñoz-Morris, M.C. García-Alonso, E. Fernández-Escalante. 2004. *In vitro* evaluation of a γ-TiAl intermetallic for potential endoprothesic applications. Intermetallics 12: 253-260.

6. Castañeda-Muñoz, D.F., P.A. Sundaram, N. Ramírez. 2007. Bone tissue reaction to Ti-48Al-2Cr-2Nb (at.%) in a rodent model: a preliminary SEM study. J Mater Sci Mater Med. 18 (7):1433-8.

7. Rivera-Denizard, O., N. Diffoot-Carlo, V. Navas, P.A. Sundaram. 2008. Biocompatibility studies of human fetal osteoblast cells cultured on gamma titanium aluminide. J Mater Sci Mater Med. 19(1): 153-158.

8. MacDonald, D.E., B.E. Rapuano, N. Deo, M. Stranick, P. Somasundaran, A.L. Boskey. 2004. Thermal and chemical modification of titanium-aluminum-vanadium implant materials: effects on surface properties, glycoprotein adsorption, and MG63 cell attachment. Biomaterials 25: 3135 – 3146.

9. Saldaña, L., N. Vilaboa, G. Vallés, J. González-Cabrero, L. Munuera. 2005. Osteoblast response to thermally oxidized Ti6Al4V alloy. J Biomed Mater Res. 73A: 97-107.

10. Saldaña, L., V. Barranco, M.C. García-Alonso, G. Vallés, M.L. Escudero, L. Munuera, N. Vilaboa. 2006. Concentration-dependent effects of titanium and aluminium ions released from thermally oxidized Ti6Al4V alloy on human osteoblasts. J Biomed Mater Res, 77A: 220-229.

11. Saldaña, L., V. Barranco, J.L. González-Carrasco, M. Rodríguez, L. Munuera, N. Vilaboa. 2007. Thermal oxidation enhances early interactions between human osteoblasts and alumina blasted Ti6Al4V alloy. J Biomed Mater Res, 81A: 334-346.

12. García-Alonso, M.C., L. Saldaña, G. Vallés, J.L. González-Carrasco, J. González-Cabrero, M.E. Martínez, E. Gil-Garay, L. Munuera. 2003. *In vitro* corrosion behaviour and osteoblast response of thermally oxidized Ti6Al4V alloy. Biomaterials 24:19-26.

13. Eisenbarth, E., D. Velten, K. Schenk-Meuser, P. Linez, V. Biehl, H. Dushner, J. Breme, H. Hildebrand. 2002. Interactions between cells and titanium surfaces. Biomolecular Engineering 19: 243-249.

14. Guleryuz H., H. Cimenoglu. 2004. Effect of thermal oxidation on corrosion and corrosion-wear behaviour of a Ti-6Al-4V alloy. Biomaterials 25: 3325-3333.

15. Fergus, J.W. 2002. Review of the effect of alloy composition on the growth rates of scales formed during oxidation of gamma titanium aluminide alloys. Mater Sci Eng. A338: 108-125.

16. ATCC® Number: CRL-11372™ Product Description. http://www.atcc.org/common/catalog/

17. Harris, S.A., R. Enger, L. Riggs, T. Spelberg. 1995. Development and characterization of a conditionally immortalized human fetal osteoblastic cell line. J Bone Miner Res, 10(2): 178-186.

18. Subramaniam, M., S.M. Jalal, D.J. Rickard, S.A. Harris, M.E. Bolander, T.C. Spelsberg. 2002. Further characterization of human fetal osteoblastic hFOB 1.19 and hFOB/ERα cells: bone formation in vivo and karyotype analysis using multicolor fluorescent in situ hybridization. J Cell Biochem, 87: 9-15.

19. Yen, M.L., C.C. Chien, I.M. Chiu, H.I. Huang, Y.C. Chen, H.I. Hu, B.L. Yen. 2007. Multilineage differentiation and characterization of the human fetal osteoblastic 1.19 cell line: a possible *in vitro* model of human mesenchimal progenitors. Stem Cells, 25:125-131.

20. Ross, M., W. Pawlina. 2006. Histology. A text and Atlas. 5th Ed. Lippincott Williams & Wilkins: Baltimore, pp. 202-217.

21. Junqueira, L.C., J. Carneiro. 2003. Basic Histology. Text and Atlas. 10th Ed. Mc Graw Hill Company: New York, pp. 141-148.

22. Jee, W.S.S. 1988. The skeletal tissues. In L. Weiss (ed) 6th ed., Cell and Tissue Biology, pp. 218-234. Urban & Schwarzenberg. Baltimore.

23. Anselme, K. 2000. Osteoblast adhesion on biomaterials. Biomaterials 21: 667-681.

24. Sommerfeldt, D. W. and C. T. Rubin. 2001. Biology of bone and how it orchestrates the form and function of the skeleton. Eur Spine J. 10: S86–S95.

25. Lim, J.Y., A. Taylor, Z. Li, E. Vogler, H. Donahue. 2005. Integrin expression and osteopontin regulation in human fetal osteoblastic cells mediated by substratum surface characteristics. Tissue Engineering 11(1/2): 20-29.

26. Liu, X., J.Y. Lim, H. Donahue, R. Dhurjati, A. M. Mastro, E. Vogler. 2007. Influence of substratum surface chemistry/energy and topography on the human fetal osteoblastic cell line hFOB 1.19: phenotypic and genotypic responses observed in vitro. Biomaterials 28: 4535-4550.

27. Piehler, H.R. 2006. Metallic biomaterials. In: S. Guelcher and J. Hollinger (eds.), An introduction to Biomaterials, pp. 291-304. Taylor & Francis: Boca Raton.

28. Davis, J.R. 2003. Handbook of materials for medical devices. ASM International: Materials Park, pp. 21-47.

29. Long M., H.J. Rack. 1998. Review. Titanium alloys in total joint replacement-a materials science perspective. Biomaterials 19: 1621- 1639.

30. Delgado-Alvarado, C. 2005. A study of the corrosion resistance of gamma Titanium Aluminide in ringer's solution, 3.5 wt% NaCl and Seawater. M. S. Thesis, University of Puerto Rico, Mayagüez.

31. Siebers, M.C., P.J. ter Brugge, X.F. Walboomers, J.A. Jansen. 2005. Integrins as linker proteins between osteoblasts and bone replacing materials. A critical review. Biomaterials 26: 137 – 146.

32. Sinha, R.K. and R.S. Tuan. 1996. Regulation of human osteoblast integrin expression by orthopedic implant materials. Bone 18(5): 451-457.

33. Ruoslahti, E. 1996. RGD and other recognition sequences for integrins. Annu. Rev. Cell Dev. Biol. 1996. 12:697–715.

34. Shah, A.K., R.K. Sinha, N.J. Hickok, R.S. Tuan. 1999. High-resolution morphometric analysis of human osteoblastic cell adhesion on clinically relevant orthopedic alloys. Bone 24(5): 499-506.

35. Villard, V., O. Kalyuzhniy, O. Riccio, S. Potekhin, T. Melnik, A. Kajava, C. Ruegg, G. Corradin. 2006. Synthetic RGD-containing α-helical coiled coil peptides promote integrin-dependent cell adhesion. J. Peptide Sci.12: 206–212.

36. Geiβler, U., U. Hempel, C. Wolf, D. Scharnweber, H. Worch, K.W. Wenzel. 2000. Collagen type I-coating of Ti6Al4V promotes adhesion of osteoblasts. J Biomed Mater Res. 51: 752-760.

37. Kornu, R., W.J. Maloney, M.A. Kelly, R. L. Smith. 1996. Osteoblast adhesion to orthopaedic implant alloys: effects of cell adhesion molecules and diamond-like carbon coating. J Orthop Res. 14: 71-87.

38. Zamir, E., B.Z. Katz, S. Aota, K.M. Yamada, B. Geiger, Z. Kam. 1999. Molecular diversity of cell-matrix adhesions. J Cell Sci. 112: 1655-1669.

39. Petit, V., V. Thiery. 2000. Focal adhesions: structure and dynamics. Biology of the Cell 92: 477- 494.

40. Wozniak, M.A., K. Modzelewska, L. Kwong, P. J. Keely. 2004. Focal adhesion regulation of cell behavior. Biochimica et Biophysica Acta 1692: 103– 119.

41. Gronowicz G., M.B. McCarthy. 1996. Response of human osteoblasts to implant materials: integrin-mediated adhesion. J Orthop Res. 14(6): 878-887.

42. Ruoslahti, E., B. Obrink. 1996. Review. Common principles in cell adhesion. Exp. Cell Res. 227: 1–11.

43. Dedhar, S. 1989. Signal transduction via the β1 integrins is a required intermediate in interleukin-1β induction of alkaline phosphatase activity in human osteosarcoma cells. Exp. Cell Res. 183: 207-214.

44. Anselme, K., B. Noel, P. Hardouin. 1999. Human osteoblast adhesion on titanium alloy, stainless steel, glass and plastic substrates with same surface topography. J Mater Sci Mater Med. 10: 815-819.

45. Anselme, K., M. Bigerelle, B. Noel, E. Dufresne, D. Judas, A. Iost, P. Hardouin. 2000. Qualitative and quantitative study of human osteoblast adhesion on materials with various surface roughnesses. J. Biomed. Mater. Res. 49: 155-166.

46. Amato, I., G. Ciapetti, S. Pagani, G. Marletta, C. Satriano, N. Baldini, D. Granchi. 2007. Expression of cell adhesion receptors in human osteoblasts cultured on biofunctionalized Poly-(ε-caprolactone) surfaces. Biomaterials 28: 3668-3678.

47. Sittig, C., M. Textor, D. Spencer, M. Wieland, P.H. Vallotton. 1999. Surface characterization of implant materials c.p. Ti, Ti-6Al-7Nb and Ti-6Al-4V with different pretreatments. J Materials Sci: Materials in Medicine. 10: 35-46.

48. Thompson, G.J. and D.A. Puleo. 1996. Ti-6Al-4V ion solution inhibition of osteogenic cell phenotype as a function of differentiation timecourse in vitro. Biomaterials 17: 1949-1954.

49. Vallés, G., P. González-Melendi, J.L. González-Carrasco, L. Saldaña, E. Sánchez-Sabaté, L. Munuera, N. Vilaboa. 2006. Differential inflammatory macrophage response to rutile and titanium particles. Biomaterials 27: 5199–5211.

50. Jacobs, J.J., N.J. Hallab, R.M. Urban, M.A. Wimmer. 2006. Wear Particles. J Bone Joint Surg Am. 88A (2 suppl): 99-102.

51. Zhu, X., J. Chen, L. Scheideler, R. Reichl, J. Geis-Gerstorfer. 2004. Effects of topography and composition of titanium surface oxides on osteoblast responses. Biomaterials 25: 4087–4103.

52. Bess, E., R. Cavin, K. Ma, J.L. Ong. 1999. Protein adsorption and osteoblast responses to heat-treated titanium surfaces. Implant Dent. 8:126-132.

53. Feng, B., J. Weng, B.C. Yang, S.X. Qu., X.D. Zhang. 2003. Characterization of surface oxide films on titanium and adhesion of osteoblast. Biomaterials 24: 4663 – 4670.

54. Kern, T., Y. Yang, R. Glover, J.L. Ong. 2005. Effect of heat-treated titanium surfaces on protein adsorption and osteoblast precursor cell line initial attachment. Implant Dent. 14: 70-76.

55. Landegren, U. 1984. Measurement of cell numbers by means of the endogenous enzyme hexosaminidase. Applications to detection of lymphokines and cell surface antigens. J Immunol Methods. 67: 379 -388.

56. Advincula, M.C., F.G. Rahemtulla, R.C. Advincula, E.T. Ada, J.E. Lemons, S.L. Bellis. 2006. Osteoblast adhesion and matrix mineralization on sol-gel-derived titanium oxide. Biomaterials 27: 2201-2212.

57. Meyer, U., T. Meyer, D.B. Jones. 1997. No mechanical role for vinculin in strain transduction in primary bovine osteoblasts. Biochem Cell Biol 75: 81-87.

58. Hanawa, T. 2004. Metal ion release from metal implants. Mater Sci Eng C 24: 745–752.

59. Hanawa, T. 1999. *In vivo* metallic biomaterials and surface modification. Mater Sci Eng A 267:260-266.

60. Sousa, S.R., M. Manuela-Bras, P. Moradas-Ferreira, M.A. Barbosa. 2007. Dynamics of fibronectin adsorption on TiO2 surfaces. Langmuir 23: 7046-7054.

61. Neitmann, M., M. Alexander, J. Brinckmann, P. Schlenke, M. Tronnier. 1999. Attachment and chemotaxis of melanocytes after ultraviolet irradiation in vitro. British J Dermatol 141: 794-801.

62. Givens, K. T., S. Kitada, A.K. Chen, J. Rothschiller, D. Lee. 1990. Proliferation of human ocular fibroblasts. Invest Ophtalmol Vis Sci 31(9): 1856-1862.

63. Okamura, A., M. Goto, T. Goto, M. Yoshinari, S. Masuko, T. Katsuki, T. Tanaka. 2001. Substrate affects the initial attachment and subsequent behavior of human osteoblastic cells (Saos-2). Biomaterials 22: 2263-2271.

64. Chen, J., S. Mwenifumbo, C. Langhammer, J.P. McGovern, M. Li, A. Beye, W.O. Soboyejo. 2007. Cell/surface interactions and adhesion on Ti-6Al-4V: effects of surface texture. J Biomed Mater Res Part B: Appl Biomater 82B: 360-373.

65. Sader, M.S, A. Balduino, G.A. Soares, R. Borojevic. 2005. Effect of three distinct treatments of titanium surface on osteoblast attachment, proliferation, and differentiation. Clin Oral Impl Res 16: 667-675.

66. Velten, D., V. Biehl, F. Aubertin, B. Valeske, W. Possart, J. Breme. 2002. Preparation of TiO2 layers on cp-Ti and Ti6Al4V by thermal and anodic oxidation and by sol-gel coating techniques and their characterization. J Biomed Mater Res 59: 18-28.

67. Anselme, K., P. Linez, M. Bigerelle, D. Le Maguer, A. Le Maguer, P. Hardouin, H.F. Hildebrand, A. Iost, J.M. Leroy. 2000. The relative influence of the topography and chemistry of Ti6Al4V surfaces on osteoblastic cell behaviour. Biomaterials 21: 1567-1577.

68. Lim, J.Y, J.C. Hansen, C.A. Siedlecki, J. Runt, H.J. Donahue. 2005. Human foetal osteoblastic cell response to polymer-demixed nanotopographic interfaces. J. R. Soc. Interface 2: 97-108.

69. May, A.L., F.M. Wood, M.L. Stoner. 2001. Assessment of adhesion assays for use with keratinocytes. Exp Dermatol 10: 62-69.

70. Zhao, G., A.L. Raines, M. Wieland, Z. Schwartz, B.D. Boyan. 2007. Requirement for both micron-and submicron scale structure for synergistic responses of osteoblasts to substrate surface energy and topography. Biomaterials 28: 2821-2829.

APPENDIX A

Standard Curves Used to Extrapolate the Number of Cells Adhered on GTi, TiV, GTi5, TiV5, GTi8 and TiV8 Surfaces Based on the Hexosaminidase Activity

A

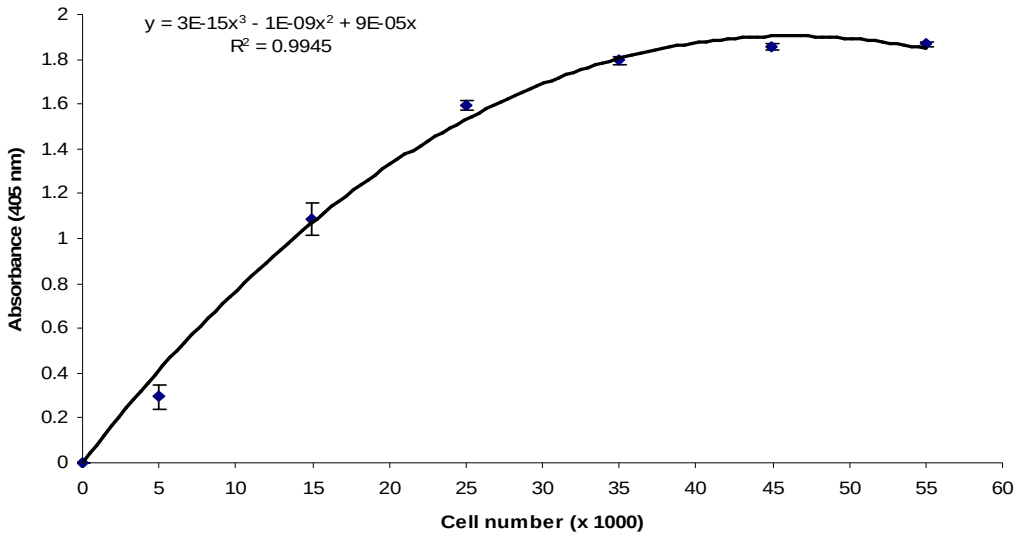

B

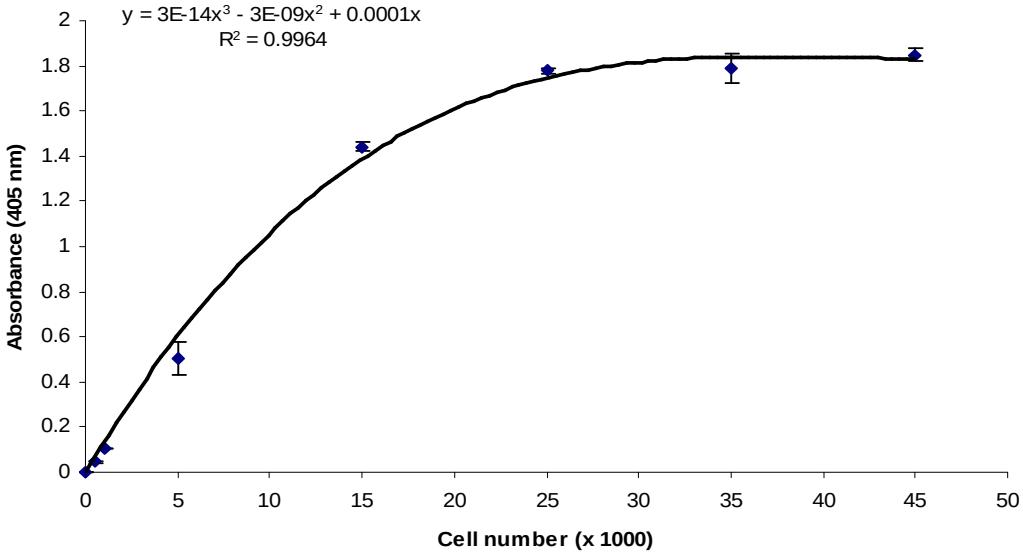

C

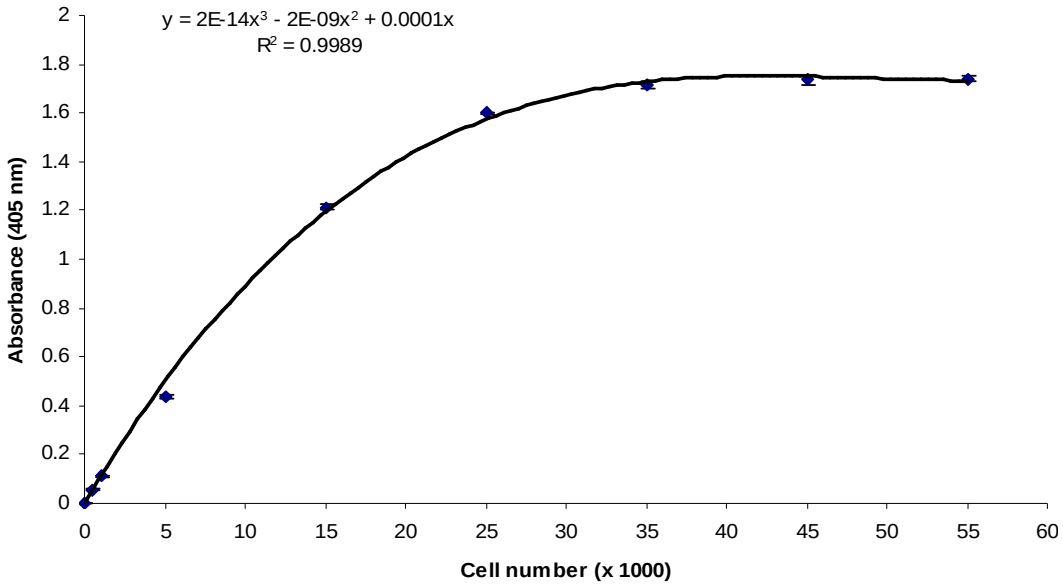

Figure 1. Standard Curves of absorbance at 405 nm versus number of cells seeded in 96-well plates. The standard curves were performed to extrapolate the number of cells attached on the different surfaces tested in experiment 1 (A), 2 (B), and 3 (C). Absorbance was read at 405 nm. Data points reflect the mean ± standard deviation (S.D.) of three wells. Most standard deviations were negligible on this scale.

Appendix A, continuation

APPENDIX B

Estimated Number of Attached Cells on gamma-TiAl and Ti-6Al-4V surfaces according to the time of incubation (1,7, and 14 days) and the Temperature of Oxidation (121[autoclaved], 500, and 800°C)

Metal	Time of incubation (days)	Temperature of oxidation (°C)	Estimated number of attached cells
gamma TiAl	1	121	4205.11
gamma TiAl	1	121	6479.665
gamma TiAl	1	121	6921.204
gamma TiAl	1	121	5339.696
gamma TiAl	1	121	8669.182
gamma TiAl	1	121	6757.251
gamma TiAl	1	121	8375.462
gamma TiAl	1	121	5006.135
gamma TiAl	1	121	2892.489
gamma TiAl	1	500	6557.239
gamma TiAl	1	500	6855.973
gamma TiAl	1	500	8682.461
gamma TiAl	1	500	7319.679
gamma TiAl	1	500	8816.179
gamma TiAl	1	500	8344.696
gamma TiAl	1	500	8919.104
gamma TiAl	1	500	10738.73
gamma TiAl	1	500	10489.9
gamma TiAl	1	800	6660.9
gamma TiAl	1	800	6842.939
gamma TiAl	1	800	8100.21
gamma TiAl	1	800	6883.706
gamma TiAl	1	800	10415.52
gamma TiAl	1	800	9481.016
gamma TiAl	1	800	13787.88
gamma TiAl	1	800	9549.781
gamma TiAl	1	800	11598.41
gamma TiAl	7	121	25466.71
gamma TiAl	7	121	28322.04
gamma TiAl	7	121	26256.84
gamma TiAl	7	121	21497.92
gamma TiAl	7	121	20494.69
gamma TiAl	7	121	20328.33
gamma TiAl	7	121	18240.58
gamma TiAl	7	121	11164.66
gamma TiAl	7	121	25496.56
gamma TiAl	7	500	29973.77
gamma TiAl	7	500	28819.48
gamma TiAl	7	500	29589.38
gamma TiAl	7	500	19576.12
gamma TiAl	7	500	18779.24

gamma TiAl	7	500	18740.01
gamma TiAl	7	500	22418.07
gamma TiAl	7	500	23729.29
gamma TiAl	7	500	26150.16
gamma TiAl	7	800	29021.06
gamma TiAl	7	800	28669.28
gamma TiAl	7	800	28794.39
gamma TiAl	7	800	19953.29
gamma TiAl	7	800	19777.18
gamma TiAl	7	800	19488.61
gamma TiAl	7	800	21445.72
gamma TiAl	7	800	20643.78
gamma TiAl	7	800	20366.05
gamma TiAl	14	121	28894.9
gamma TiAl	14	121	29557.56
gamma TiAl	14	121	29764.84
gamma TiAl	14	121	18904.9
gamma TiAl	14	121	18831.89
gamma TiAl	14	121	19163.02
gamma TiAl	14	121	26702.69
gamma TiAl	14	121	29794.37
gamma TiAl	14	121	31541.23
gamma TiAl	14	500	29300.73
gamma TiAl	14	500	29686.92
gamma TiAl	14	500	29609.23
gamma TiAl	14	500	18655.71
gamma TiAl	14	500	18798.94
gamma TiAl	14	500	18884.92
gamma TiAl	14	500	30708.63
gamma TiAl	14	500	31690.44
gamma TiAl	14	500	31869.66
gamma TiAl	14	800	29071.69
gamma TiAl	14	800	29686.92
gamma TiAl	14	800	29764.84
gamma TiAl	14	800	18591.52
gamma TiAl	14	800	18858.35
gamma TiAl	14	800	18911.58
gamma TiAl	14	800	30886.57
gamma TiAl	14	800	30560.57
gamma TiAl	14	800	32258.52
Ti-6Al-4V	1	121	3658.17
Ti-6Al-4V	1	121	4131.777
Ti-6Al-4V	1	121	9453.765
Ti-6Al-4V	1	121	6663.194
Ti-6Al-4V	1	121	6554.293
Ti-6Al-4V	1	121	5771.692
Ti-6Al-4V	1	121	7982.745
Ti-6Al-4V	1	121	8545.789
Ti-6Al-4V	1	121	7256.79
Ti-6Al-4V	1	500	9412.061

Ti-6Al-4V	1	500	10554
Ti-6Al-4V	1	500	5408.654
Ti-6Al-4V	1	500	9002.439
Ti-6Al-4V	1	500	9115.579
Ti-6Al-4V	1	500	9273.722
Ti-6Al-4V	1	500	11021.82
Ti-6Al-4V	1	500	10520.86
Ti-6Al-4V	1	500	12574.85
Ti-6Al-4V	1	800	2939.612
Ti-6Al-4V	1	800	1883.645
Ti-6Al-4V	1	800	6350.699
Ti-6Al-4V	1	800	4473.511
Ti-6Al-4V	1	800	4182.956
Ti-6Al-4V	1	800	4078.723
Ti-6Al-4V	1	800	2052.528
Ti-6Al-4V	1	800	3050.424
Ti-6Al-4V	1	800	3426.812
Ti-6Al-4V	7	121	28346.69
Ti-6Al-4V	7	121	28619.4
Ti-6Al-4V	7	121	29377.52
Ti-6Al-4V	7	121	19510.39
Ti-6Al-4V	7	121	21962.06
Ti-6Al-4V	7	121	19532.23
Ti-6Al-4V	7	121	19593.94
Ti-6Al-4V	7	121	23524.09
Ti-6Al-4V	7	121	23703.57
Ti-6Al-4V	7	500	30157.96
Ti-6Al-4V	7	500	28869.74
Ti-6Al-4V	7	500	32392.02
Ti-6Al-4V	7	500	19066.83
Ti-6Al-4V	7	500	18918.26
Ti-6Al-4V	7	500	19114.76
Ti-6Al-4V	7	500	25604.76
Ti-6Al-4V	7	500	25523.58
Ti-6Al-4V	7	500	26287.63
Ti-6Al-4V	7	800	694.232
Ti-6Al-4V	7	800	256.284
Ti-6Al-4V	7	800	233.94
Ti-6Al-4V	7	800	323.12
Ti-6Al-4V	7	800	757.064
Ti-6Al-4V	7	800	435.669
Ti-6Al-4V	7	800	332.199
Ti-6Al-4V	7	800	525.493
Ti-6Al-4V	7	800	658.618
Ti-6Al-4V	14	121	24871.51
Ti-6Al-4V	14	121	29816.92
Ti-6Al-4V	14	121	29816.92
Ti-6Al-4V	14	121	18805.52
Ti-6Al-4V	14	121	18772.69
Ti-6Al-4V	14	121	18898.24

Ti-6Al-4V	14	121	29823.72
Ti-6Al-4V	14	121	29941.2
Ti-6Al-4V	14	121	31720.3
Ti-6Al-4V	14	500	29249.67
Ti-6Al-4V	14	500	30000.11
Ti-6Al-4V	14	500	29712.87
Ti-6Al-4V	14	500	18628.55
Ti-6Al-4V	14	500	18891.57
Ti-6Al-4V	14	500	18871.62
Ti-6Al-4V	14	500	30235.61
Ti-6Al-4V	14	500	30294.61
Ti-6Al-4V	14	500	31243.26
Ti-6Al-4V	14	800	222.773
Ti-6Al-4V	14	800	122.388
Ti-6Al-4V	14	800	77.845
Ti-6Al-4V	14	800	282.385
Ti-6Al-4V	14	800	292.56
Ti-6Al-4V	14	800	100.301
Ti-6Al-4V	14	800	251.259
Ti-6Al-4V	14	800	80.128
Ti-6Al-4V	14	800	231.065

Appendix B, continuation

APPENDIX C

1. ANOVA for Number of attached cells versus Metal, Time of incubation, and Temperature of oxidation

Factor	Type	Levels	Values
Metal	fixed	2	gamma TiAl, Ti-6Al-4V
Time of incubation (days)	fixed	3	1, 7, 14
Temperature of oxidation	fixed	3	121, 500, 800

Analysis of Variance for Number of attached cells

Source	DF	SS	MS	F	P
Metal	1	1271906861	1271906861	78.39	0.000
Time of incubation (days)	2	6715835489	3357917745	206.96	0.000
Temperature of oxidation	2	2797312262	1398656131	86.20	0.000
Metal*Time of incubation (days)	2	407759989	203879994	12.57	0.000
Metal*Temperature of oxidation	2	3219793202	1609896601	99.22	0.000
Time of incubation (days)* Temperature of oxidation	4	1008444005	252111001	15.54	0.000
Metal*Time of incubation (days)* Temperature of oxidation	4	700898171	175224543	10.80	0.000
Error	144	2336435925	16225249		
Total	161	18458385904			

S = 4028.06 R-Sq = 87.34% R-Sq(adj) = 85.85%

2. ANOVA: Number of attached cells versus Metal, Time of incubation, and Temperature of oxidation without data of cell attachment on surfaces thermally oxidized at 800°C (GTi8, TiV8)

Factor	Type	Levels	Values
Metal	fixed	2	gamma TiAl, Ti-6Al-4V
Time of incubation (days)	fixed	3	1, 7, 14
Temperature of oxidation	fixed	2	121, 500

Analysis of Variance for Number of attached cells

Source	DF	SS	MS	F	P
Metal	1	13249574	13249574	0.69	0.409
Time of incubation (days)	2	7229605905	3614802953	187.53	0.000
Temperature of oxidation	1	78246128	78246128	4.06	0.047
Metal*Time of incubation (days)	2	11110936	5555468	0.29	0.750
Metal*Temperature of oxidation	1	264276	264276	0.01	0.907
Time of incubation (days)* Temperature of oxidation	2	20412920	10206460	0.53	0.591
Metal*Time of incubation (days)* Temperature of oxidation	2	2548756	1274378	0.07	0.936
Error	96	1850459085	19275615		
Total	107	9205897580			

S = 4390.40 R-Sq = 79.90% R-Sq(adj) = 77.60%

3. Tukey 95% Simultaneous Confidence Intervals All Pairwise Comparisons among Levels of Time of incubation (days)

```
Individual confidence level = 98.07%

Time of incubation (days) =  1 subtracted from:

Time of
incubation
(days)      Lower  Center  Upper  -------+---------+---------+---------+--
 *7          13595   16024  18454                          (---*--)
*14          16006   18436  20865                             (--*---)
                                 -------+---------+---------+---------+--
                                        0      7000     14000     21000

* There are significant differences between time of incubation (days) when 0 is not
included in the simultaneous confidence interval. In this case, the number of cells
attached on disks at day 1 is less compared to the number of cells attached on disks
after 7 and 14 days of incubation.

Time of incubation (days) =  7 subtracted from:

Time of
incubation
(days)      Lower  Center  Upper  -------+---------+---------+---------+--
14            -18    2411   4841         (--*---)
                                 -------+---------+---------+---------+--
                                        0      7000     14000     21000
```

4. Tukey 95% Simultaneous Confidence Intervals All Pairwise Comparisons among Levels of Temperature of oxidation

```
Individual confidence level = 95.00%

Temperature of oxidation = 121 subtracted from:

Temperature
of
oxidation    Lower  Center  Upper  ----+---------+---------+---------+-----
500          -1838    1702   5243         (-------------*-------------)
                                  ----+---------+---------+---------+-----
                                  -2500         0      2500      5000
```

APPENDIX D

Multiple Contrasts of Hypotheses Using 95% Bonferroni Intervals of Confidence of the Estimate Number of Cells Attached on GTi, TiV, GTi5, TiV5, GTi8 and TiV8 Surfaces for Each Time Point

Table 1. Multiple contrasts of hypotheses of the estimate number of cells attached on the different surfaces tested after 1 day of incubation

Treatments	*Contrast	∇Standard error	♣95% simultaneous confidence intervals	
			Lower Limit	Upper Limit
GTi -TiV	-596.891	1898.845	-6915.51	5721.723
GTi -TiV5	-3581.98	1898.845	-9900.59	2736.636
GTi-GTi5	-2453.09	1898.845	-8771.7	3865.529
GTi-GTi8	-3186.02	1898.845	-9504.63	3132.595
GTi-TiV8	2467.476	1898.845	-3851.14	8786.09
TiV-GTi5	-1856.19	1898.845	-8174.81	4462.42
TiV-TiV5	-2985.09	1898.845	-9303.7	3333.527
TiV-GTi8	395.9592	1898.845	-5922.66	6714.574
TiV-TiV8	3064.367	1898.845	-3254.25	9382.982
GTi5-TiV5	-1128.89	1898.845	-7447.51	5189.721
GTi5-GTi8	-732.934	1898.845	-7051.55	5585.68
GTi5-TiV8	4920.561	1898.845	-1398.05	11239.18
TiV5-GTi8	395.9592	1898.845	-5922.66	6714.574
TiV5-TiV8	6049.454	1898.845	-269.16	12368.07
GTi8-TiV8	5653.495	1898.845	-665.119	11972.11

*Each contrast represents the difference in the mean number of attached cells between two treatments

∇ The standard error was calculated using the formula $\sqrt{2\left(\frac{MSE}{r}\right)}$, where MSE= Mean Squared Error obtained from the Factorial ANOVA, r = replications.

♣ The formula to calculate the Bonferroni simultaneous confidence intervals was

Contrast $\pm t[1-\alpha/2g,(r-1)abc]\sqrt{2\left(\frac{MSE}{r}\right)}$, where α=0.05, g= number of contrasts evaluated (in this case were 15),r = replications, a= levels of factor a, b= levels of factor b, c= levels of factor c.

Table 2. Multiple contrasts of hypotheses of the estimate number of cells attached on the different surfaces tested after 7 days of incubation

Treatments	Contrast	Standard error	95% simultaneous confidence intervals	
			Lower Limit	Upper Limit
GTi -TiV	-1877.95	1898.845	-8196.57	4440.66
GTi -TiV5	-3185.25	1898.845	-9503.86	3133.367
GTi-GTi5	-2278.58	1898.845	-8597.19	4040.036
GTi-GTi8	-1210.12	1898.845	-7528.73	5108.497
GTi-TiV8	21450.19	1898.845	*15131.57	27768.8
TiV-GTi5	-400.624	1898.845	-6719.24	5917.99
TiV-TiV5	-1307.29	1898.845	-7625.91	5011.321
TiV-GTi8	667.8366	1898.845	-5650.78	6986.451
TiV-TiV8	23328.14	1898.845	*17009.53	29646.76
GTi5-TiV5	-906.669	1898.845	-7225.28	5411.945
GTi5-GTi8	1068.461	1898.845	-5250.15	7387.075
GTi5-TiV8	23728.77	1898.845	*17410.15	30047.38
TiV5-GTi8	1975.13	1898.845	-4343.48	8293.744
TiV5-TiV8	24635.43	1898.845	*18316.82	30954.05
GTi8-TiV8	22660.31	1898.845	*16341.69	28978.92

* There are significant differences between treatments when 0 is not included in the simultaneous confidence interval

Table 3. Multiple contrasts of hypotheses of the estimate number of cells attached on the different surfaces tested after 14 days of incubation

Treatments	Contrast	Standard error	95% simultaneous confidence intervals	
			Lower Limit	Upper Limit
GTi -TiV	76.48956	1898.845	-6242.12	6395.104
GTi -TiV5	-441.385	1898.845	-6760	5877.229
GTi-GTi5	-672.197	1898.845	-6990.81	5646.417
GTi-GTi8	-603.908	1898.845	-6922.52	5714.707
GTi-TiV8	25721.63	1898.845	*19403.02	32040.25
TiV-GTi5	-748.687	1898.845	-7067.3	5569.927
TiV-TiV5	-517.875	1898.845	-6836.49	5800.74
TiV-GTi8	-680.397	1898.845	-6999.01	5638.217
TiV-TiV8	25645.14	1898.845	*19326.53	31963.76
GTi5-TiV5	230.8123	1898.845	-6087.8	6549.427
GTi5-GTi8	68.28989	1898.845	-6250.32	6386.904
GTi5-TiV8	26393.83	1898.845	*20075.22	32712.44
TiV5-GTi8	-162.522	1898.845	-6481.14	6156.092
TiV5-TiV8	26163.02	1898.845	*19844.4	32481.63
GTi8-TiV8	26325.54	1898.845	*20006.93	32644.15

* There are significant differences between treatments when 0 is not included in the simultaneous confidence interval

Appendix D, continuation